Case Studies in Construction Materials 20 (2024) e02822

Contents lists available at ScienceDirect

Case Studies in Construction Materials

journal homepage: www.elsevier.com/locate/cscm

# Evaluating lithium slag for geopolymer concrete: A review of its properties and sustainable construction applications

Sanjida Khair , SM Arifur Rahman , Faiz Uddin Ahmed Shaikh *, Prabir Kumar Sarker

*School of Civil and Mechanical Engineering, Curtin University, Perth, Australia*

ARTICLE INFO

*Keywords:*
Lithium slag geopolymer
Alkali activation
Thermomechanical activation
Fresh properties
Mechanical properties
Durability
Microstructure

ABSTRACT

This comprehensive review paper evaluates lithium slag (LS) as a promising precursor for geopolymer concrete, focusing on its workability, strength, durability, and microstructure. In the context of sustainable construction, LS emerges as a vital alternative to conventional cementitious materials, primarily due to the environmental concerns associated with cement production, such as substantial greenhouse gas emissions and air pollution. Geopolymer technology utilizes alkali activators and aluminosilicate-rich materials, offers a reduced environmental footprint and shows comparable performance to traditional cement-based concrete. In particular, LS has gained attention for its potential as an aluminosilicate precursor material in geopolymer concrete. This review investigated the recent advancements in LS-based geopolymers, exploring various processing techniques like mechanical activation, calcination, and chemical treatment to optimize LS geopolymerisation and enhance early strength development. The incorporation of binary/ternary aluminosilicate material is also discussed, aiming to improve crucial properties such as workability, strength, durability, and microstructure. The needs for comprehensive research into LS-based geopolymers to achieve their full potential in sustainable construction, promoting an environmentally friendly approach and contribution to a circular economy in the construction industry are highlighted.

## 1. Introduction

Concrete is a fundamental construction material composed of cement, aggregates, water, and additives, and renowned for its strength and durability [1]. Concrete is continuously increasing in significance with each passing day as a pivotal contributor to the economy, and it is primarily cement that assumes the central and indispensable role in the production of concrete [2–4]. However, the production of cement left behind high amount of carbon footprint by generating $CO_2$, $SO_2$, $NO_x$, and dust into the atmosphere [5–9]. The environmental impact of cement production, characterized by substantial greenhouse gas emissions and air pollution, has spurred interest in seeking sustainable alternatives [10]. Geopolymer, a cement-free binder formed through the reaction between alkali activators and aluminosilicate-rich materials, has emerged as a promising substitute for traditional cement-based concrete, offering improved performance and reduced environmental footprint [11–14].

Geopolymer represents the cutting-edge and most innovative approach for replacing cement in the construction industry, showcasing superior performance and effectiveness in comparison to conventional practices [15]. Geopolymer is produced by a chemical reaction involving aluminosilicate compounds and an alkali-activator, with fly ash, ground granulated blast furnace slag, or silica fume

* Correspondence to: Professor, School of Civil and Mechanical Engineering, Curtin University, Perth, Australia.
*E-mail address:* shaikhfa@rocketmail.com (F.U.A. Shaikh).

https://doi.org/10.1016/j.cscm.2023.e02822
Received 21 August 2023; Received in revised form 2 December 2023; Accepted 20 December 2023
Available online 22 December 2023

being common aluminosilicate sources [16–19]. In the presence of an alkaline solution (sodium hydroxide or potassium hydroxide), the aluminosilicate compounds dissolve and activate amorphous precursors, leading to the formation of an N-(C)-A-S-H gel through cross-linking of aluminate and silicate species [20–22]. This amorphous gel acts as the main binding agent in geopolymerisation, resulting in geopolymer products with outstanding mechanical properties, fire and chemical resistance, and a reduced carbon footprint compared to traditional cement-based concrete [23–26]. Recent studies have explored the use of chemically activated materials like fly ash (FA), ground granulated blast furnace slag (GGBFS), silica fume (SF), and rice husk to produce FA-based and GGBFS-based geopolymers, which demonstrate resilience and improved chemical and fire resistance [27–30].

Among the alternative materials investigated for geopolymer production, Lithium Slag (LS) has gained attention due to its potential as a supplementary cementitious material and source material for geopolymer concrete [31]. The proper management and reuse of LS can be challenging due to environmental concerns when it is disposed in landfills, as it has the potential to cause pollution. Improper disposal of LS in landfills can lead to the leaching of harmful substances, such as fluoride and sulfate, into the surrounding land and water, posing a significant environmental threat [32,33]. This challenge is exacerbated by the growing generation of LS waste globally, with various countries like China, Australia, France, USA, Germany, Malaysia, Japan, and Singapore importing significant amounts of lithium in 2020 [34], as shown in Fig. 1. The improper management and disposal of LS not only pose environmental risks through potential leaching of harmful substances but also squander a valuable resource that could contribute to sustainable construction materials [5,31,35,36]. Therefore, to promote sustainable practices, effective techniques for utilizing, and repurposing LS, such as in geopolymer concrete production need to be explored.

The utilisation of LS in geopolymer concrete production represents a significant contribution towards sustainable construction practices in the pursuit of a circular economy. The circular economy model emphasizes the reduction of waste and the continual use of resources, aligning perfectly with the repurposing of LS, a by-product of lithium refinery [37]. As illustrated in Fig. 1, significant amounts of lithium are produced globally which consequently produces LS, presenting a substantial waste management challenge. When LS is discarded in landfills, it poses severe environmental risks due to the leaching of harmful substances like heavy metals and sulfate [38]. By using LS as precursor material for geopolymer concrete, not only this hazardous waste is diverted from landfills, but also is recycled in geopolymer, thereby reducing reliance on traditional cement [5]. This approach exemplifies the principle of circular economy helping resource regeneration and waste minimisation. Furthermore, the enhanced durability and mechanical properties of geopolymer concrete made by LS contribute to durable construction materials, reducing the need for frequent repairs or replacements [39]. The extended lifecycle of LS as a construction material further reinforces the circular economy model by maximising resource efficiency and minimising waste generation [5]. Ultimately, the incorporation of LS into geopolymers will not only mitigate environmental impacts but also foster a sustainable, resource-efficient approach in the construction industry, aligning with the principles of a circular economy.

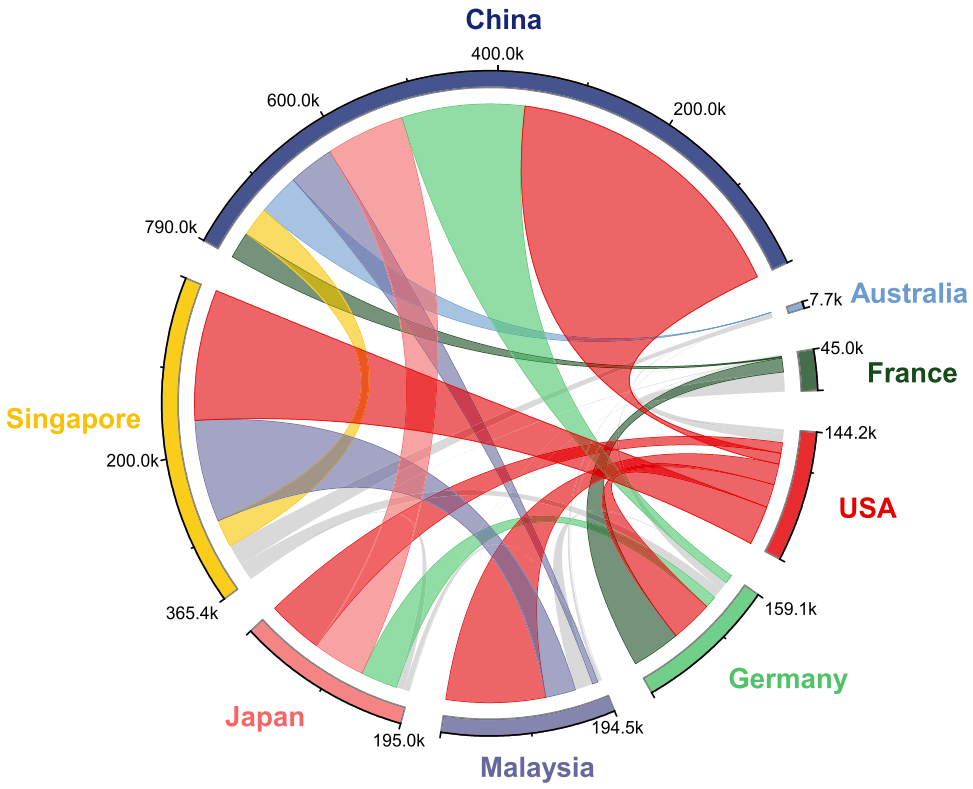


**Fig. 1.** Major lithium battery importing scenario by countries in 2020 (combined and reproduced) [34].

To address the environmental concerns associated with LS waste and fully harness the potential of LS-based geopolymers, it is crucial to explore recent advancements in processing techniques and understand their properties [36,38,40–52]. This review paper aims to provide a comprehensive analysis of the recent advances in LS-based geopolymers and their properties. By examining the latest research findings and characterizations, this review seeks to guide future research and promote the practical application of LS-based geopolymers in the construction industry. This study will explore various processing techniques, such as micronisation, calcination, and chemical treatment, to optimize LS geopolymerisation, and enhance the material's early strength development. Additionally, the incorporation of binary/ternary materials will be discussed to further improve properties like workability, strength, durability, and microstructure development in LS geopolymer products. This study will drive innovation and promote the environmentally friendly use of LS in geopolymers, offering a more sustainable approach to concrete construction. By repurposing LS waste through geopolymerisation, this study aims to contribute to a circular economy in the construction industry and pave the way for an eco-friendlier and resource-efficient future.

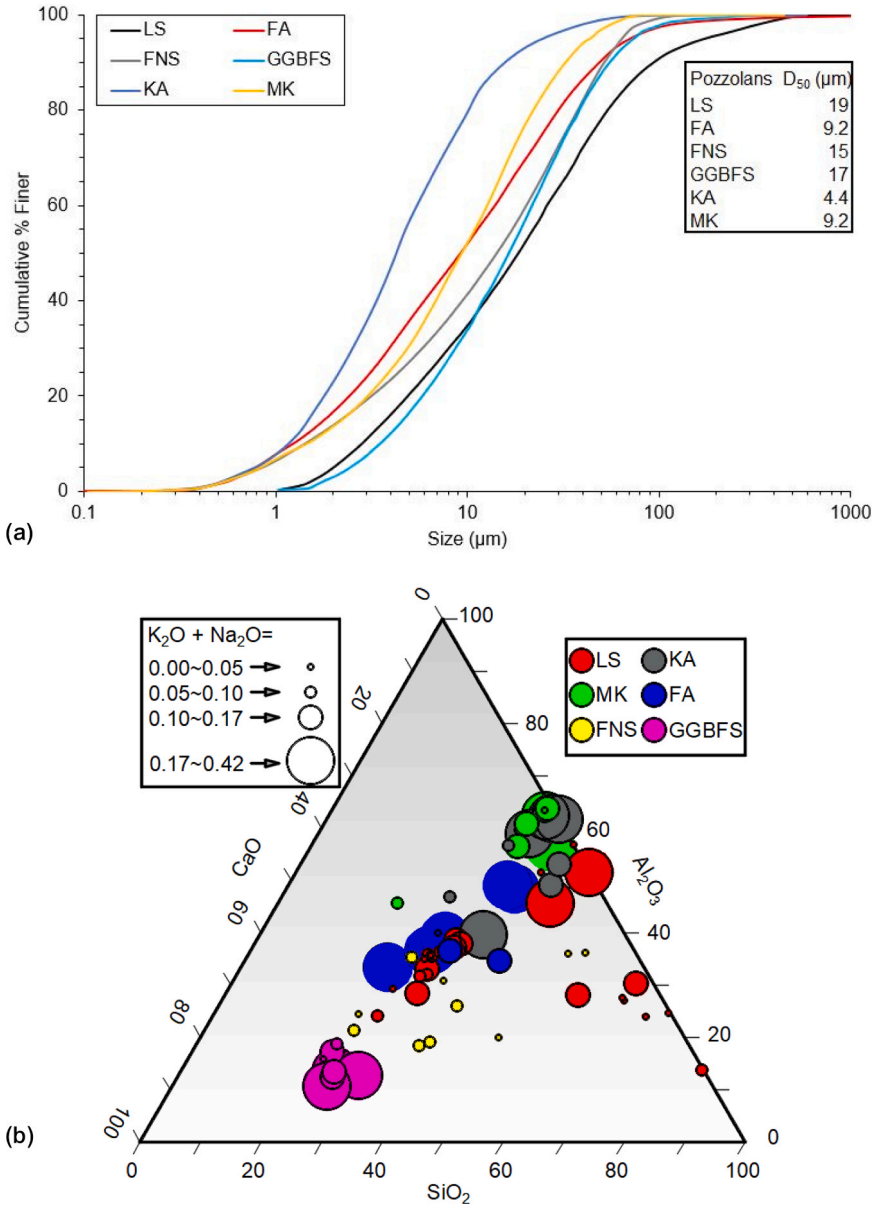


**Fig. 2.** Grain size of LS [53], FA [49], FNS [54], GGBFS [53], KA [49], and MK [55] with median particle size (combined only) (a) and (b) major oxide compositions in four axes ($SiO_2$, $Al_2O_3$, CaO, and $Na_2O+K_2O$) of different materials used as a binder: LS [16,17,31,35,36,40,43,48–52,56–82], KA [83–92], MK [93–102], FA [103–109], FNS [110–118], and GGBFS [119–127] (combined and reproduced). Here, FNS, KA, and MK represents ferronickel slag, kaolin, and metakaolin, respectively.

## 2. Physiochemical and microstructural properties of lithium slag

The physiochemical properties of LS have an important influence on geopolymerisation. Rahman et al. [5] reported that $D_{10}$, $D_{50}$ and $D_{90}$ of LS varies from 0.13–20, 0.3–171, and 0.66–180 μm, respectively. The variation of grain size of commonly used pozzolans as a geopolymer reported by different authors along with their corresponding $D_{50}$ are shown in Fig. 2(a). The median grain size of LS is maximum (19 μm) among the commonly used pozzolans [53]. The fineness of the LS ranges from 400–1800 $m^2$/kg, and the dry density was found 2450–2500 kg/$m^3$. The LOI of LS at 750°C was found to vary from 0 to 33% [5]. The main oxide compositions of LS and

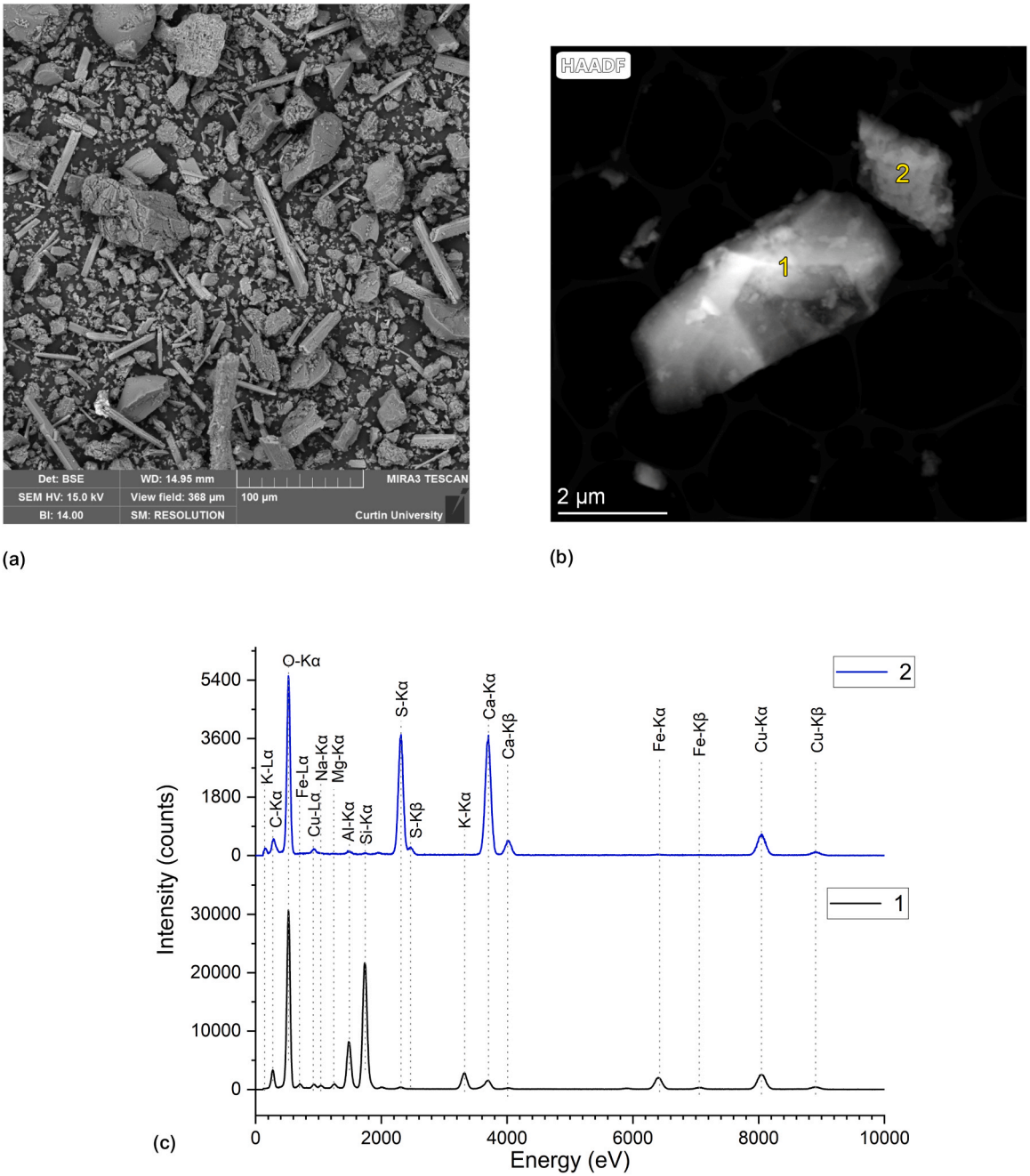


**Fig. 3.** Backscattered electron image of LS to identify the microstructural texture of the grains [82] (a), HAADF image of typical LS grains (b) [128], and (c) STEM-EDS at positions 1 and 2, as shown in Fig. 3(b) [128].

conventional aluminosilicate pozzolans for the production of geopolymers are presented in Fig. 2(b). Particularly, the average silica content of LS is higher compared to the conventional supplementary cementitious materials (SCMs), while the calcium content is lower in the same comparison.

A backscattered electron microscopy (BSE) image of LS particles is shown in Fig. 3(a) [82]. The LS grains are irregular shaped, composed of dense rod-like gypsum particles, and crystalline [3]. The shiny glassy particles in the phase composition have a negative impact when activated for the geopolymerisation reaction [73]. Researchers recommended that thermo-mechanical treatment on LS induces amorphousness and reactivity [45,48]. The LS was also characterised in scanning transmission electron microscope (STEM) and the observed microstructure is shown in a high annular angular dark field image in Fig. 3(b) [128]. The characteristic LS grains 1 and 2 were analysed in super electron diffraction spectra (EDS) at 200 kV to analyse the elemental composition, as shown in Fig. 3(c). The elemental compositions of locations 1 and 2 indicated the presence of amorphous aluminosilicate and bassanite phases, respectively. It is seen that reactive Ca, K, and Fe are present in the aluminosilicate phase that may participate in the early stage of the geopolymerisation reaction and can form amorphous intermediate and amorphous hydration products.

The diffraction patterns of LS were studied by several researchers and developed the mineralogical composition of LS. In general, spodumene, anorthite, quartz, and gypsum are the major mineralogical composition of LS [36,41,43–45,48,49,52]. Calcining LS at 300, 500, and 700°C provided significant variation in the amorphous and mineralogic composition [36,44,45,48], as shown in Fig. 4. Specifically, raw LS contained 17–28% amorphousness and calcining at 700°C increased the amorphousness to 51–82% [45,48]. In addition, one and two hours grounding increase the amorphousness to 34–38% [45], while 300–500°C heating raise the amorphousness to 21–38% [48]. Therefore, calcination was found most effective technique for increasing amorphousness among calcination-grounding, grounding-calcination, and grounding. The TESCAN integrated mineral analyser (TIMA) micrographs of raw and 700°C calcined LS are shown in Fig. 4 to compare the composition of different minerals representing amorphous aluminosilicate. Specifically, the major minerals spodumene and anorthite derived from aluminosilicate phase were highly reduced after calcination at 700°C, and the produced glassy phase increased the reactivity of LS [45]. Besides, thermogravimetry of LS is found to be very helpful in understanding the conversion of the amorphous phase from crystals and the total mass loss due to LOI. It is found that crystalline phase of LS particles transforms to amorphous phase at 250–650°C, with a relative mass loss of 2.3–3.3%, and the total LOI at 1000 °C was 11.7–13% [36,48–51].

The properties of LS can vary significantly depending on the source. The major producers of lithium are Australia, China, Chile, Argentina, and United States of America. The variety of factors, including the mineral source of the lithium, the extraction and processing methods used, and local geological conditions influence LS properties. Specifically, the chemical compositions of LS can vary based on the type of lithium-bearing ores. Lithium is extracted from the minerals spodumene, lepidolite, petalite, or zinnwaldite [128]. Different extraction and processing methods, which may vary regionally based on technology and environmental regulations, can lead to different types of salt residues in the slag. Primarily, the lithium rich minerals are mixed with sulfate salts and lime, chlorine, or carbonate salts, followed by roasting at 850–1150 °C to form β-spodumene from α-spodumene [129–131]. Therefore, potential variations in the oxide concentrations in the LS changes, and further processing for environmental disposal also changes the concentration of S, Mg, Al, Si, K, Na, and Fe bearing minerals. Researchers mostly reported that higher concentration of $SO_3$ in LS restricts geopolymerisation reaction [132]. On the contrary, researchers also reported that roughly 10.7% $Na_2O$ content in the LS

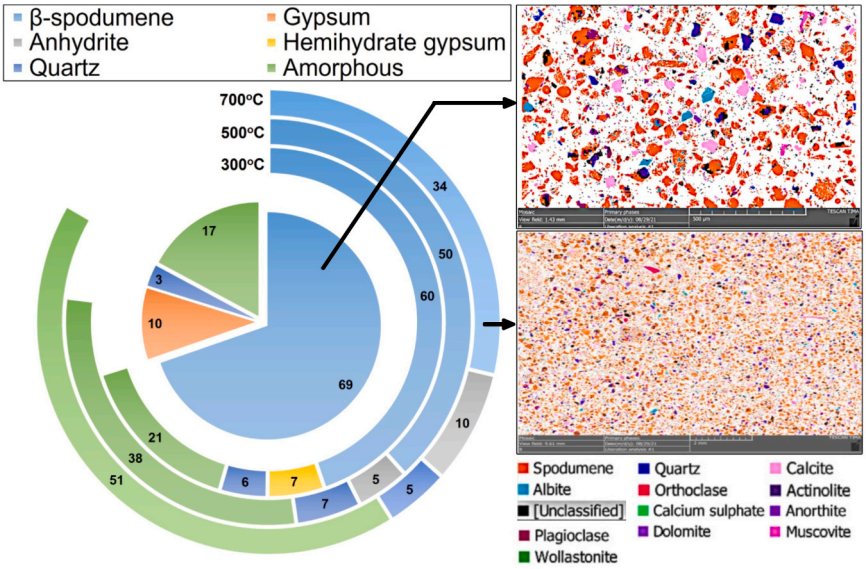


**Fig. 4.** Changes in the amorphousness and chemical composition of LS at 300, 500, and 700°C. The centre pie chart shows the chemical composition and amorphousness of raw LS. TIMA micrographs of LS at raw and after 700°C [44,45].
All the numbers in relative wt% (reproduced from [48]).

generated in the Jiangxi Province of China [75]. On the other hand, the texture, grain size, and porosity of LS can vary depending on the processing techniques employed, and these are often adapted to mineral characteristics. The LS from China and Australia regions with fine-grained ore are finer, while LS from north and south American sources with coarser ore are more granular [133]. The concentration of heavy metals present in LS are influenced by the original ore and the processing methods [38]. LS processed in Australia possess higher levels of impurities like sulphate or heavy metals, and affect the slag's usability in the production of cement and geopolymer concrete [5]. This may be influenced not only by the slag itself but also by the local environmental regulations and the

**Table 1**
Major oxide compositions, calcination temperature, LS percentage, precursor materials, alkaline activators, water-binder ratio (w/b), and summary of literature review.

| References | $SiO_2 + CaO + Al_2O_3$ (%) | LS Calcination temp. (°C) | LS (%) | Precursors | Activators | w/b | Summary |
|---|---|---|---|---|---|---|---|
| Liu et al.[48] | 87.83 | - | 80-100 | $SiO_2$ | SS+SH | 0.50 | Pre-heating facilitated the reactivity of LS |
| | | 300 (2 h) | 85 | | | | |
| | | 500 (2 h) | 85 | | | | |
| | | 700 (2 h) | 85 | | | | |
| Liu et al.[36] | 87.83 | - | 85 | - | SS+SH | 0.50 | The Si-O-Al bond increases with alkaline activation of LS which enhances geopolymerisation reaction |
| Perumal et al. [52] | 91.31 | - | 100 | - | SS+SH | 0.34 | Geopolymer could not be formed from 100% LS after calcining at 750 °C |
| | | 750 (2 h) | 100 | | | | |
| | | 900 (2 h) | 100 | | | | |
| Karrech et al. [49] | 95.10 | - | 50-100 | GGBFS, FA | SS+SH | 0.46 | LS retards curing of the geopolymer |
| | | 750 (48 h) | 50 | GGBFS | | | |
| Lemougna et al.[70] | 91.30 | 700 (2 h) | 90-100 | LDS | SH+SC | 0.24 | SH performed better than SC as an activator |
| | | 800(2 h) | 90-100 | | | | |
| | | 900(2 h) | 90-100 | | | | |
| Wang et al. [40] | 87.83 | 700 (2 h) | 92-100 | $Na_2B_4O_7$ | SS+SH | 0.65 | Setting times of LS geopolymer mortar increased with the lowering of activator dosage |
| Luo et al.[43] | 75.13 | - | 50-100 | GGBFS | SS+SH | 0.30 | 70% LS geopolymer significantly improved fresh, mechanical, and hydration properties |
| Shah et al. [41] | 65.66 | - | 60-100 | GGBFS | SS | 0.30 | GGBFS improved reactivity and rapid hardening of LS based geopolymer at ambient curing |
| Karrech et al. [51] | 86.80 | - | 0-75 | FA, GGBFS | SS+SH+ SC | - | 25% LS induced strength with sodium silicate activator |
| Karrech et al. [50] | 86.80 | - | 0-50 | FA, GGBFS | SS+SH | - | Superior workability and strength achieved by 10% LS geopolymer |
| Li et al.[42] | 86.16 | - | 0-60 | MK | SS+SH | 0.52 | Low activator dosage and LS % are required for strength and dense microstructure |
| Shen et al. [135] | 75.60 | - | 50-85 | FA | SS+SH | 0.57-0.62 | 50% LS with different precursors enhanced strength and setting times |
| | | | 50 | FA, SF | | | |
| | | | 50 | FA, SF, GGBFS | | | |
| Javed et al. [132] | 83.15 | 700 | 72.5 | Borate | SS+SH | 0.40 | Thermo-mechanical treatment enhances amorphousness of LS to be used as a geopolymer precursor |
| Javed et al. [44] | 83.15 | 700 | 0-100 | FA | SS+SH | 0.40 | FA and SF densified N-(C)-A-S-H gel in LS geopolymer by restricting $SO_4^{2-}$ ions in the pore solution |
| | | | 60-100 | SF | | | |
| Shen et al. [137] | 75.60 | - | 30.6 | FA, SF, GGBFS, CG | SS+SH | 0.40 | LS geopolymer containing FA, SF, and GGBFS precursors enhanced workability and strength |
| Tian et al. [53] | - | - | 10-30 | GGBFS | SS+SH | 0.35 | Calcium fluoride enhances workability of LS geopolymer but drops strength |
| Fan et al.[38] | 85.53 | - | 10-30 | MK, NS | SS+SH | - | LS geopolymer containing MK and NS immobilise heavy metals Cu, Cr, and Pb |
| Luo et al.[47] | 79.40 | - | 50 | GGBFS | SS+SH<br>SH+CH<br>SH+CC | 0.40 | CC activator increased the reaction degree of the hardened paste by promoting C-A-S-H gel |
| Dai et al.[46] | 79.26 | 1450 | 30-70 | LZT | SS+SH | 0.36 | Heat curing enhances the solidification of the geopolymer pared from activated LS and LZT |
| Guo and Wang [136] | 70.42 | - | 0-40 | GGBFS, MK | SH | 0.70 | 20% LS optimised the energy consumption and cost for the production of geopolymer by using GGBFS and MK precursors |

Here, CG, LZT, SS, CC, CH, and SC represents coal gangue, lead-zinc slag, $Na_2SO_4$, $CaCO_3$, $Ca(OH)_2$, and $Na_2CO_3$, respectively.

methods used for slag disposal or recycling. Therefore, these regional differences are important for the effective management and utilization of LS.

In conclusion, LS can play significant physical and chemical roles in the production of geopolymer, and an eco-friendly alternative to Portland cement. The physical characteristics of LS include the particle size and shape, and ground LS particles influence the density and porosity of the final geopolymer product. The fine particles of LS can fill voids within the geopolymer matrix, leading to a denser and more uniform microstructure. This improves the mechanical properties and durability of the geopolymer. In addition, finer slag particles can enhance the workability, reducing segregation and bleeding. On the other hand, the source of amorphous aluminosilicate in LS influences its chemical role in the production of geopolymer. These aluminosilicates undergo a chemical reaction with alkaline activators to form the geopolymer matrix. The LS can maintain pH of the geopolymer mix from the dissolution of aluminosilicate precursors and alkaline activators. The reactive aluminosilicate phase of LS can influence the setting time and reactivity of the geopolymer mix.

## 3. Mix design and comparative analysis of the properties of LS geopolymer

The evaluation of LS in geopolymer-based materials has received considerable interests in recent research, emphasizing its role in sustainable construction. This section presents a critical comparison and synthesis of various studies, offering a deeper understanding of the behaviour LS geopolymers. A summary of the mix designs and results reported in previous studies incorporating LS is given in Table 1.

Liu et al. [36,48] and Karrech et al. [49] investigated the basic properties of LS as a geopolymer component. Liu et al. [36,48] identified the lower pozzolanic activity of LS compared to FA and GGBFS. However, the study noted that the reactivity of LS could be improved through heat and chemical activation, enhancing its microstructure and early compressive strength. In contrast, Karrech et al. [49] found that LS, as a sole binder, exhibited low reactivity and did not harden efficiently. Similar findings were reported in the study of Perumal et al. [52]. The study suggested its use as an energy-efficient alternative to KA, especially when combined with phosphate tailings, improved its compressive strength and binding efficiency. This study emphasizes the necessity of combining LS with more reactive aluminosilicate materials to fully exploit its potential.

Lemougna et al. [70] demonstrated the versatility of LS in producing low-temperature ceramics in combination with feldspar sand and ladle slag (LDS), and Sodium Hydroxide (SH) as an effective fluxing agent, leading to higher compressive strength and lower water absorption. This study expands the application of LS, indicating its potential beyond traditional geopolymer formulations. Wang et al. [40] and Luo et al. [43] focused on the practical challenges in LS geopolymer production. Wang et al. [40] explored the issues related to the adhesive nature of silicate-based geopolymers, emphasizing the importance of activator dosage and modulus in controlling setting and hardening. Luo et al. [43] noted that while LS negatively impacted fluidity, it significantly improved compressive strength when kept below 70% concentration.

Shah et al. [134] and Javed et al. [44,45] furthered this exploration by studying the effects of GGBFS content and thermo-mechanical processing on LS geopolymer as suggested in the study of Liu et al. [36,48]. Shah et al. [134] discovered that increasing GGBFS content reduced setting time and improved flowability and compressive strength under ambient temperature curing. Javed et al. [44,45] emphasized the importance of thermo-mechanical processing in enhancing compressive strength of LS geopolymer, suggesting a correlation between alkaline activator content, NaOH molarity, and improved reaction kinetics. Later, Shen et al. [135] investigated the effects of aluminium powder and reclaimed material (RM) substitution on geopolymer foams based on LS. The study showed that incorporation of SF and GGBFS optimized the gel structure and improved compressive strength of LS geopolymer as suggested in Javed et al. [44,45].

Tian et al. [53], Fan et al. [38], and Dai et al. [46] investigated the effects of additional components like calcium fluoride (FL), nickel slag, and fine-grained tailings on LS geopolymers. Tian et al. [53] reported a decrease in flexural and compressive strengths with the addition of these materials, indicating a need for careful mix optimization. Fan et al. [38] demonstrated how a combination of nickel slag (NS) and LS could improve compressive strength and immobilize heavy metals, offering a sustainable option for tailings solidification. Dai et al. [46] showed that LS could be effectively used with fine-grained tailings to create geopolymers with reasonable strength and low porosity. Guo and Wang [136] used MK and GGBFS to prepare LS geopolymer paste mixes, and the optimum cost and total energy consumption for the production of the geopolymers were demonstrated from the strength, setting times, fluidity, and hydration heat properties. Similarly, Li et al. [55] employed response surface method (RSM) to design geopolymer mixes and found that 10% LS promoted early strength development in MK-based geopolymers.

In conclusion, while these studies collectively highlight the potential of LS in sustainable building materials and waste management, they also underscore the need for precise optimization of LS activation and formulation. This comparative analysis reveals a common theme: the success of LS in geopolymer applications hinges on its combination with other reactive materials and careful adjustment of processing conditions. Future research should thus focus on refining these combinations and conditions to maximize the sustainable and practical applications of LS geopolymers.

## 4. Fresh properties

### 4.1. Fluidity

Table 2 presents a summary of the fresh state properties of LS geopolymer. Shah et al. [41] observed that geopolymer paste with 100% LS exhibited reduced flowability, but gradual improvement in flow diameter was recorded with the addition of GGBFS.

Specifically, a geopolymer mix with 60% GGBFS and LS achieved a flow diameter of 300 mm. This improvement in flowability with GGBFS can be attributed to its lower water demand compared to LS. The irregular shape and high surface roughness of LS particles contribute to inter-particle friction, further reducing the flowability of the geopolymer mix. Luo et al. [43] investigated on the fluidity of LS geopolymer paste and found that a mix with 50% GGBFS and LS exhibited a fluidity of 203 mm. The study showed a reduction in fluidity with an increase in LS content, as a 50% GGBFS LS geopolymer paste produced 150% more flowability than a 100% LS paste. However, increasing the activator modulus from 1.0 to 2.0 induced only a negligible effect on fluidity, with approximately 14.3% improvement. In contrast, at an activator dose of 2.5, fluidity slightly reduced due to the saturation of LS pores with the activator, leading to decreased flowability. Subsequent studies by Karrech et al. [50,51] investigated the flow test of LS geopolymer pastes using a slump cone and recommended the use of SS to enhance the workability of LS geopolymers with FA. The flowability of geopolymer pastes with 50% LS was found to be reduced to 110 mm compared to 10% LS, which exhibited a flowability of 130 mm. In other investigations, Shen et al. [137] achieved a flow diameter of 193 mm using a multi-pozzolan geopolymer system with 28% LS. Similarly, Tian et al. [53] reported a flow diameter of 200 mm by incorporating 70% GGBFS in LS geopolymer. Lastly, Luo et al. [47] achieved a flow diameter of 190 mm for a 50% GGBFS composite LS geopolymer. Therefore, the addition of GGBFS and SS can significantly improve the flowability of LS geopolymer pastes, making them more suitable for various practical applications. The activator modulus has a minor impact on the fluidity of the geopolymer mix, while the LS content and the choice of other pozzolanic materials also influence the flowability of the geopolymer paste. These findings provide valuable insights for optimizing the workability and performance of LS-based geopolymer materials.

### 4.2. Setting times

This research has investigated the setting times in LS geopolymers, and influence of LS content, activator ratios, and additive types based on previous research, as shown in Table 2. The setting characteristics of LS geopolymers are pivotal as they determine the material's workability and suitability for specific applications. Karrech et al. [50] identified a direct relationship between the LS content and the SS:SH ratio with the setting times. As the LS content increased from 10% to 50%, the initial setting time (IST) extended from 19 min to 65 min, and the final setting time (FST) from 68 to 125 min. The slower reaction, attributed to the presence of gypsum in LS, prolongs these setting times.

Conversely, Shah et al. [41] observed that substituting LS with high GGBFS content reduced the setting times. This can be explained by the faster dissolution of CaO in GGBFS compared to $SiO_2$ and $Al_2O_3$ in LS, facilitating earlier nucleation during the geopolymerisation process. Notably, a 40% GGBFS replacement in LS resulted in the shortest IST and FST, at 140 and 480 min,

**Table 2**
Fresh state and hydration properties of LS geopolymer from different studies.

| References | LS Calcination temp. (°C) | LS (%) | Precursors | Activators | R = $SiO_2$/$Na_2O$ | w/b | Fluidity (mm) | IST (min) | FST (min) | Cum. Heat at 24 h (J/g) | Shear yield stress (Pa) |
|---|---|---|---|---|---|---|---|---|---|---|---|
| Liu et al.[48] | - | 80 | $SiO_2$ | SS+SH | 1.78 | 0.50 | - | - | - | 48 | - |
| | 300 | 85 | | | 1.07 | | - | - | - | 149 | - |
| | 500 | 85 | | | 1.07 | | - | - | - | 122 | - |
| | 700 | 85 | | | 1.07 | | - | - | - | 62 | - |
| Liu et al.[36] | - | 85 | - | SS+SH | 1.78 | 0.50 | - | - | - | 79 | - |
| Wang et al. [40] | 700 | 100 | - | SS+SH | 2.00 | 0.65 | - | 16 | 37 | 58 | - |
| | | 92 | $Na_2B_4O_7$ | | 1.50 | | - | 73 | 84 | 43 | 2.9 |
| Luo et al. [40] | - | 50 | GGBFS | SS+SH | 2.00 | 0.30 | 203 | - | - | 405 | - |
| Shah et al. [41] | - | 60 | GGBFS | SS | 0.91 | 0.30 | 300 | 140 | 480 | - | - |
| Karrech et al. [51] | - | 10 | FA, GGBFS | SS+SH+ SC | 2.50 | - | 130 | 19 | 68 | - | - |
| Karrech et al. [50] | - | 50 | FA, GGBFS | SS+SH | 2.00 | - | 110 | 65 | 125 | - | - |
| Shen et al. [135] | - | 50 | FA | SS+SH | 1.00 | 0.60 | - | 85 | 238 | - | - |
| Javed et al. [44] | 700 | 50 | FA | SS+SH | 1.16 | 0.40 | - | 19 | 38 | | - |
| | | 60 | SF | | 1.16 | | - | 16 | 24 | - | - |
| Shen et al. [137] | - | 28 | FA, SF, GGBFS, CG, RM | SS+SH | 1.00 | 0.40 | 193 | 225 | - | - | - |
| Tian et al. [53] | - | 30 | GGBFS | SS+SH | 1.50 | 0.35 | 200 | 22 | 30 | - | 40 |
| Luo et al. [47] | - | 50 | GGBFS | SS+SH | 1.00 | 0.40 | 192 | - | - | - | - |
| | | | | SH+CH | 1.00 | | 190 | - | - | - | - |
| | | | | SH+CC | 1.00 | | 189 | - | - | - | - |
| Guo and Wang [136] | - | 40 | GGBFS, MK | SH | - | 0.70 | 175 | 198 | 216 | 290 | 23 |

respectively. Further, Wang et al. [40] explored the role of the alkali activator and its dosage, revealing that higher activator modulus and specific $Na_2O_{eq}$ content ranges affect setting times [138–140]. Moreover, the addition of sodium tetraborate, used as a retarder, increased both IST and FST.

Additionally, the impact of Fly Ash (FA) and Silica Fume (SF) was investigated. While Shen et al. [135] reported significant retardation with 50% FA, leading to IST and FST of 85 and 238 min, respectively, Javed et al. [44] found that 50% FA had a minimal effect compared to 40% SF. For the latter, the IST and FST were considerably shorter, at 16 and 24 min, respectively. Lastly, Shen et al. [137] observed that a mix with 28% LS in a multi-precursor system resulted in a high IST of 238 min, demonstrating the substantial influence of LS content and mix composition on setting behaviour. These findings emphasize the complex interplay between LS content, activator dosage, and additives in determining the setting characteristics of LS geopolymers. Understanding these interactions is vital for formulating geopolymers with desired setting times and optimizing their application in various construction applications.

### 4.3. Heat of hydration

Table 2 also presents the cumulative heat generated by geopolymer pastes containing 50–92% LS, with varying combinations of w/b, M, and pozzolan, observed over a 24-hour period. The incorporation of LS resulted in reduced total hydration heat for geopolymers prepared with conventional pozzolans. Luo et al. [40] investigated the hydration behaviour of a 50% GGBFS LS composite geopolymer, recording a maximum 405 J/g hydration heat at 24 h, whereas an 8% sodium tetraborate LS geopolymer paste generated 48 J/g hydration heat at 24 h [40]. LS's physiochemical properties, such as low amorphousness, higher $D_{50}$, and sulfate content, were found to retard the total hydration heat of geopolymers. In another study by Liu et al. [48], heat evolution in LS geopolymer pastes with 0–20% $SiO_2$ was examined for 24 h. Three heat generation peaks were observed, with the first two occurring concurrently. Higher SiO2 content and a low dose of alkali activator reduced heat evolution due to bond breaking and conversion to Si-OH and Al-OH species [141]. Furthermore, the study reported that non-calcined LS at 80–85% concentration produced 48–79 J/g hydration heat at 24 h, while 85% calcined LS at 300, 500, and 700 °C produced 149, 122, and 62 J/g hydration heat, respectively [36,48]. Wang et al. [40] found that an 8% sodium tetraborate LS geopolymer paste produced 43 J/g hydration heat, whereas a geopolymer made solely with LS produced 58 J/g in the same comparison. Moreover, Luo et al. [43] reported that increasing LS concentration in the production of GGBFS-LS composite geopolymer reduced the total hydration heat, with the 50% GGBFS LS geopolymer producing 405 J/g hydration heat at 24 h. The nature of the hydration peaks was found to be similar to the results of previous studies [36,48].

### 4.4. Rheology

Several researchers [40,53,136] performed the rheology test on the LS geopolymers, and the summary of their findings is presented in Table 2. Firstly, Tian et al. [53] used Bingham model [142] to idealise 10–30% LS incorporated geopolymer mixes by using the alkaline activators SS and SH, respectively. The yield stress of the control mix was 62.6 Pa with 100% GGBFS, while increasing LS content in the mix gradually reduced the yield stress to half of the control for 20% LS content. However, the yield stress 8 Pa for 30% LS mix compared to 20% LS. The slight increase in the yield stress may be due to the concentration of mineral admixture to maintain same fluidity of 20% and 30% LS mixes. The study also reported that the predicted shear stress from the Bingham model provided good fitting with the experimentally obtained shear stress and the correlation coefficient $R^2$ was higher than 0.97. In this study, the initial setting time of the control mix was 15.5 min, and initial setting time was increased to 22 min at 30% LS mix. Wang et al. [40] used 0–8% $Na_2B_4O_7$ and water-binder ratio of 0.65 to prolong the setting times and therefore the yield stresses of the mixes were highly reduced accordingly. A borax dosage of 3% increased the 20 times yield stress compared to the control, however, 5–8% borate dosage significantly reduced the yield stress and initial setting was delayed by 18 and 38 min compared to 3% borate mix. Therefore borate dosage extends the setting time than the conventional preparation of LS geopolymer prepared by Tian et al. [53]. The study concludes that plastic yield stress of the LS geopolymer with 3–8% borate can be fitted with Krieger-Dougherty model [143]. Lastly, Guo and Wang [136] used Herschel-Bulkley model for the idealisation of the shear stress versus shear rate of the 10–40% LS mixes at liquid-solid ratio of 0.7. The study indicated that using LS as a partial replacement of MK with 60% GGBFS contained system consistently reduced the setting times. The initial setting time of the control mix (60% GGBFS with 40% MK) was 51.8 h, while the yield stress of the mix was 56.19 Pa. The initial setting time was reduced to 216 min at 40% LS addition, while the yield stress was reduced to 22.64 Pa. The exponent of Herschel-Bulkley model was less than 1, and this indicated higher shear thinning of the geopolymer pastes and the coefficient of correlation $R^2$ was greater than 0.99 for mixes. The studies on the rheology of LS geopolymers shows that varying LS content, liquid-binder ratio, and additives like borate significantly affect yield stress and setting times, correlating well with the Bingham, Krieger-Dougherty, and Herschel-Bulkley models.

## 5. Mechanical properties

### 5.1. Compressive strength

The studies on the compressive strength of LS geopolymers present a complex picture and influenced by various factors like calcination temperature, LS percentage, and the type of activators and additives used [144–147]. These factors collectively impact the mechanical properties and ultimate usability of LS geopolymers in practical applications.

Liu et al. [48] explored the effects of calcination at different temperatures on LS geopolymers. Their study showed that as the calcination temperature increased (300 °C, 500 °C, and 700 °C), there was a corresponding enhancement in the compressive strength.

For instance, at 500 °C and 700 °C, the compressive strength reached 38.9 MPa and 50.0 MPa at 7 days, and 42.5 MPa and 52.2 MPa at 28 days, respectively. This enhancement is attributed to the amorphous nature and reduced β-spodumene concentration due to higher calcination temperatures. Perumal et al. [52] took this a step further by calcining LS at even higher temperatures (750 °C and 900 °C). However, these extreme temperatures did not yield any compressive strength, suggesting that there might be a threshold beyond which further calcination could be detrimental to the structural integrity of the geopolymers [49,52]. Karrech et al. [49] demonstrated the importance of combining LS with other materials. When LS was mixed with 50% GGBFS, the composite achieved a high compressive strength of 51.0 MPa and 85.2 MPa at 7 and 28 days, respectively. This indicates the synergistic effect of combining LS with GGBFS, which significantly enhances the compressive strength. Further, calcination of LS at 750 °C in combination with GGBFS also resulted in impressive strength gains, reaching 56.5 MPa and 88.1 MPa at 7 and 28 days, respectively.

Wang et al. [40] and Luo et al. [43] focused on the role of activators in LS geopolymers. Wang et al. [40] found that using different modulus activators influenced the compressive strength. At a modulus activator of 2.00 and LS calcined at 700 °C, they recorded strengths of 16.1 MPa and 27.5 MPa at 7 and 28 days, respectively. Luo et al. [43] confirmed this trend, showing that an increase in activator modulus could enhance the compressive strength of LS geopolymers. Shah et al. [41] proposed an optimal mix design with 60% LS and 40% GGBFS, leading to a compressive strength of 52.4 MPa and 56.3 MPa at 7 and 28 days, respectively. This mix design represents a balance between LS content and additives, optimizing strength while maintaining workability. Karrech et al. [50,51] and Li et al. [42] focused on varying the content of LS and other additives. While Karrech et al. [50,51] found lower strengths with increased LS content, Li et al. [42] achieved high compressive strengths (55.0 MPa and 67.5 MPa at 7 and 28 days) with 20% LS and MK, emphasizing the importance of balancing LS with suitable additives.

Shen et al. [135,137] explored the combination of LS with FA, SF, and GGBFS in different ratios. Their results varied, indicating the nuanced effect of each additive on the compressive strength of LS geopolymers. Fan et al. [38] and Luo et al. [43] also investigated the effect of various parameters on LS geopolymer compressive strength. The authors indicated that a higher modulus activator reduced the nucleation and restricts the formation of N-C-A-S-H by increasing $SiO_2/Na_2O$ ratio [148–150]. Dai et al. [46] and Guo and Wang [136] examined LS geopolymers at extreme calcination temperatures and with different additive combinations. Dai et al. [46] calcined

**Table 3**
Mechanical properties of LS geopolymer from different studies.

| Ref. | LS Calcination temp. (°C) | LS (%) | Precursors | Activators | R | w/b | Curing type | Compressive strength (MPa) | | Flexural strength (MPa) | |
|---|---|---|---|---|---|---|---|---|---|---|---|
| | | | | | | | | 7 days | 28 days | 7 days | 28 days |
| Liu et al.[48] | - | 80 | $SiO_2$ | SS+SH | 1.78 | 0.50 | 70 °C | 12.9 | 12.8 | - | - |
| | 300 | 85 | | | 1.07 | | (12 h) | 13.5 | 12.8 | - | - |
| | 500 | 85 | | | 1.07 | | | 38.9 | 42.5 | - | - |
| | 700 | 85 | | | 1.07 | | | 50.0 | 52.2 | - | - |
| Perumal et al. [52] | 750 | 100 | - | SS+SH | 2.52 | 0.34 | Ambient | 0.0 | 0.0 | | |
| | 900 | 100 | - | | 2.52 | | | 0.0 | 0.0 | - | - |
| Karrech et al. [49] | - | 100 | - | SS+SH | 2.00 | 0.46 | Ambient | 0.0 | 0.0 | - | - |
| | - | 75 | GGBFS | | | | | 20.0 | 34.8 | - | - |
| | - | 50 | GGBFS | | | | | 51.0 | 85.2 | - | - |
| | - | 50 | GGBFS, FA | | | | | 23.2 | 38.2 | - | - |
| | 750 | 50 | GGBFS | | | | | 56.5 | 88.1 | - | - |
| Wang et al.[40] | 700 | 100 | - | SS+SH | 2.00 | 0.65 | 70 °C | 16.1 | 27.5 | 4.8 | 8.0 |
| | | 92 | $Na_2B_4O_7$ | | 1.50 | | (12 h) | 15.0 | 22.5 | 4.9 | 5.9 |
| Luo et al.[43] | - | 50 | GGBFS | SS+SH | 2.00 | 0.30 | Ambient | 22.3 | 32.2 | - | - |
| Shah et al.[41] | - | 80 | GGBFS | SS | 0.91 | 0.30 | Ambient | 18.1 | 23.8 | 5.5 | 6.0 |
| | - | 60 | GGBFS | SS | | | | 52.4 | 56.3 | 2.2 | 2.6 |
| Karrech et al. [51] | - | 10 | FA, GGBFS | SS+SH+ SC | 2.50 | - | Ambient | 14.5 | 33.7 | - | - |
| Karrech et al. [50] | - | 50 | FA, GGBFS | SS+SH | 2.00 | - | Ambient | 3.0 | 5.0 | - | - |
| Li et al.[42] | - | 20 | MK | SS+SH | 1.50 | 0.52 | Ambient | 55.0 | 67.5 | - | - |
| | - | 40 | | | | | | 49.1 | 58.7 | - | - |
| Shen et al.[135] | - | 50 | FA | SS+SH | 1.00 | 0.60 | Ambient | 17.5 | 18.3 | - | - |
| | - | 50 | FA, SF, GGBFS | | | | | 26.4 | 31.3 | - | - |
| Shen et al.[137] | - | 31 | FA, SF, GGBFS, CG | SS+SH | 1.00 | 0.40 | 30 °C (4 h) | 4.5 | - | - | - |
| | | 28 | FA, SF, GGBFS, CG, RM | | | | | 2.8 | - | - | - |
| Tian et al.[53] | - | 30 | GGBFS | SS+SH | 1.50 | 0.35 | Ambient | - | 50.1 | - | - |
| Fan et al.[38] | - | 30 | MK | SS+SH | 1.50 | | Ambient | 34.0 | 45.0 | - | - |
| Luo et al.[47] | - | 50 | GGBFS | SS+SH | 1.00 | 0.40 | Ambient | - | 22.5 | - | - |
| | | | | SH+CH | 1.00 | | | - | 29.1 | - | - |
| | | | | SH+CC | 1.00 | | | - | 36.2 | - | - |
| Dai et al.[46] | 1450 | 50 | LZT | SS+SH | | 0.36 | 75 °C (12 h) | 36.4 | 45.6 | - | - |
| Guo and Wang [136] | - | 40 | GGBFS, MK | SH | - | 0.70 | Ambient | - | 14.8 | - | - |

LS at 1450 °C, achieving compressive strengths of 36.4 MPa and 45.6 MPa at 7 and 28 days. Guo and Wang [136] combined GGBFS and MK with LS, achieving a compressive strength of 14.8 MPa at 28 days. In summary, the mechanical properties of LS geopolymers are significantly influenced by calcination temperature, LS content, and the type and ratio of additives and activators used. Optimal compressive strength is achieved through a delicate balance of these factors, which varies depending on the specific application requirements of the geopolymer. The studies collectively provide valuable insights into optimizing LS geopolymer formulations for superior mechanical performance.

### 5.2. Flexural strength

The flexural strength of LS as a partial substitute for natural pozzolan in the preparation of geopolymer is shown in Table 3, notable studies by Wang et al. [40] and Shah et al. [41] have scrutinized the flexural strength aspects. Shah et al. [41] conducted research to evaluate the flexural strength of geopolymer compositions incorporating LS. A 20% GGBFS LS composite geopolymer showed commendable flexural strength, indicating 5.7 and 6 MPa at 7 and 28 days, respectively. Nonetheless, it is crucial to acknowledge that a range of 30–40% GGBFS mixtures experienced reduced flexural strength, attributed to the emergence of micro-cracks within the system. In a parallel exploration, Wang et al. [40] investigated the flexural strength of LS geopolymer formations and found a high flexural strength at an activator modulus of 1.5.

Interestingly, this parameter held a more pronounced influence on flexural strength compared to the volume of LS. Notably, the flexural strength was notably unaltered when the activator modulus was adjusted to 2.0. This emphasizes the critical role that activator concentration plays in influencing the flexural strength outcomes [151–154]. Furthermore, Wang et al. found that alkali dosage contributed to the modulation of flexural strength. Specifically, the study demonstrated that the maximum flexural strength achieved was 8.2 MPa at 28 days for an alkali dosage corresponding to 18% $Na_2O_{eq}$. Intriguingly, it was observed that the borate dosage had an adverse impact on flexural strength, indicating the delicate balance that must be struck to optimize flexural performance [40].

## 6. Durability performance

### 6.1. Drying shrinkage

In general, drying shrinkage is one of the key durability properties of geopolymer that mainly depends upon the pozzolan, activators combination and dosage, admixtures, additives, aggregates, and curing condition [144–147]. Wang et al. [40] shown that drying shrinkage of the control LS geopolymer was 2400 με with an activator modulus of 1.0, while 8% borate dosage reduced 56% drying shrinkage at 28 days. The B-O-Al-O-Si structure retained high moisture and reduced gel pore tensile stress to reduce drying shrinkage [155,156]. Later, Shah et al. [41] reported that increase in the GGBFS content in the LS geopolymer reduced long-term drying shrinkage (as a function of length) and mass loss. An incorporation of 10–40% GGBFS in LS composite geopolymer reduced 4.8–12% mass loss and 1–1.4% length change, respectively at 110 days. The improvement in controlling drying shrinkage via crack mitigation was attributed to the reduction in permeable pores through enhanced geopolymerisation [157] and the reduction in the volume of micro-pores and mesopores through the filler effect of unreacted finer LS particles [158,159]. Karrech et al. [50] studied the shrinkage strain of 0–40% LS mixes at molar ratios of 1.5, 2, and 2.5. The study reported that the shrinkage strain of the control specimen was roughly 0.003–0.0035 after 16 weeks of curing. The shrinkage strain of the 10–40% LS mixes was slightly increased with increased activator molar ratio. However, the shrinkage strain consistently reduced with the addition of LS in the mix, and the shrinkage strain was 0.0014 for 40% LS mix at 1.5 molar ratio. In conclusion, drying shrinkage is a critical durability property of geopolymers which is influenced by various factors like pozzolan types, activator combinations, and curing conditions. Studies have shown that additives like borate and GGBFS significantly reduce drying shrinkage in LS geopolymers by retaining moisture, reducing pore tension, and enhancing geopolymerisation, and mitigates cracks and reduces micro and mesopores.

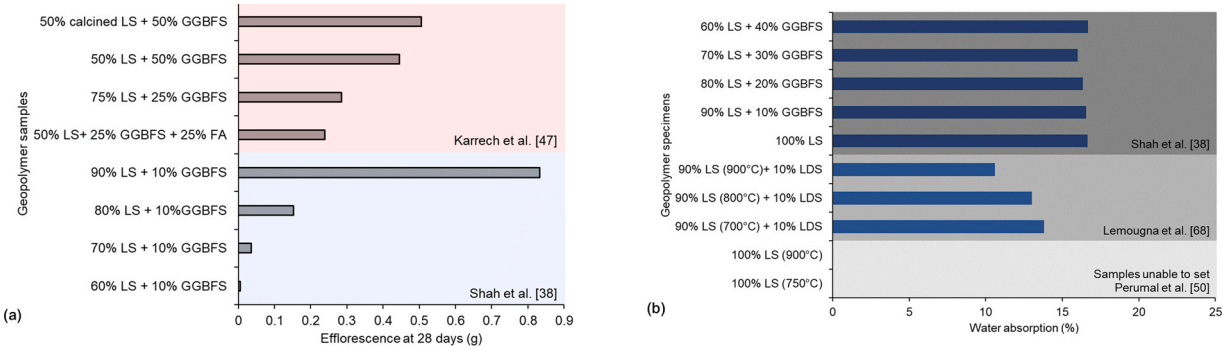


**Fig. 5.** Efflorescence of partially incorporated LS geopolymers [41,49] (combined only) (a) and (b) variation of water absorption percentage and permeable pore volume for different LS geopolymer specimens [41,52,70] (combined only).

### 6.2. Efflorescence

Several researchers investigated the efflorescence property of LS geopolymer and some of their results are shown in Fig. 5(a). Karrech et al. [49] found that GGBFS-LS composite geopolymer produced higher efflorescence compared to FA-LS and MK-LS geopolymers. A 25% GGBFS LS sample produced 0.29 g salt at 28 days. Surprisingly, calcined LS produced higher efflorescence than the raw. A 50% GGBFS LS geopolymer produced 0.447 g salt at 28 days, while 0.507 g slat with calcined LS in the same comparison. In contrast, suing 25% FA with LS (50%) and GGBFS (25%) reduced efflorescence and 0.245 g was reported at 28 days. The presence of FA in geopolymer formed higher volume of N-(C)-A-S-H gel from the reaction between activator and FA. The N-(C)-A-S-H gel arrests salt formation and binds the alkali more strongly [160,161]. Shah et al. [41] also reported a reduced efflorescence with increased GGBFS in LS geopolymers, as demonstrated in Fig. 5(a). Samples with 10% GGBFS produced 0.83 g slat on 28 days. This increase in salt extrusion is related to a higher volume of permeable pores in the specimen [58]. Moreover, the samples with higher GGBFS showed negligible efflorescence as complete geopolymerisation resulted in a more compact and chemically stable gel structure. Samples containing 20–30% GGBFS observed a significant reduction in efflorescence in LS geopolymer. No efflorescence was reported for the sample with 40% GGBFS and 60% LS at both early and late ages of curing. Wang et al. [40] showed that alkali reduction proportionally reduces strength and stimulates efflorescence in LS-based geopolymer by using multiple pozzolan in a mixture. Efflorescence may occur due to the subsistence of dissolution equilibrium of raw aluminosilicate in alkaline silicate solutions [43,162]. The above discussion indicates that an appropriate mix proportion of geopolymer and proper production techniques are important to overcome the common problems of geopolymer such as drying shrinkage, efflorescence, and long-term durability.

### 6.3. Water absorption

Reduction of capillary pores and air void provide a denser matrix of geopolymer that consequent to low permeability and ensures high durability of geopolymer [163]. Size, volume, and connectivity of pores are the principal governing factors of the compressive strength, thermal conductivity, and permeability of geopolymer [164]. The variation of the water absorption of different LS content geopolymer is shown in Fig. 5(b). It is seen that 100% calcined LS geopolymer could not set from Perumal et al. [52]. Later, Lemougna et al. [70] studied the water absorption of 10% LDS LS composite geopolymer at different activator contents. The study found that LS calcination from 700–900 °C reduces the water absorption from 13.8% to 10.6%. Calcination increases in the amorphousness and reactivity of LS, and reduced the capillary and large avoids reducing the water absorption. Shah et al. [41] also found that increased GGBFS has an affirmative influence on the durability performance of LS geopolymer, as less water absorption and permeable pore volume were noticed. The reduction in the water absorption could be linked to enhanced geopolymerisation reaction and a reduction of C-A-S-H gel increased higher bound water content than N-A-S-H gel [165,166] [167]. Pangdaeng et al. [168] also found that reduction of the volume of permeable pores improved the compressive strength and water absorption. Therefore, the reduction in capillary pores and air voids in LS geopolymers leads to a denser matrix with lower permeability and higher durability. Studies indicate that factors like LS calcination and the addition of GGBFS effectively decrease water absorption and pore volume in geopolymers, enhancing their compressive strength and durability due to increased amorphousness, reactivity, and improved geopolymerisation reactions.

### 6.4. Sulfate resistance

Wang et al. [40] studied the effects of adding 3–8% $Na_2B_4O_7$ to lime-stone (LS) mixes, observied their compressive strength and

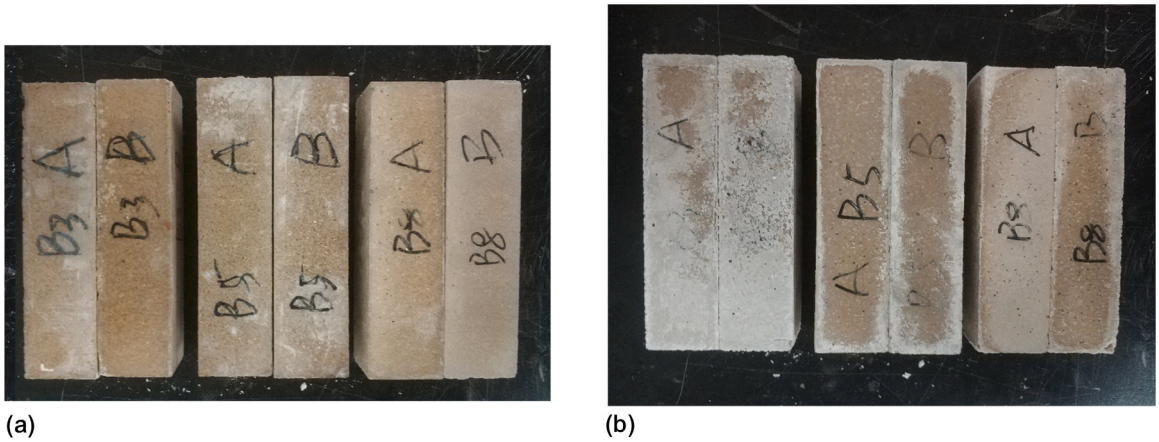


**Fig. 6.** Physical condition of the 3–8% $Na_2B_4O_7$ LS geopolymer sulfate attacked samples exposed in 5 g/L $MgSO_4$ (a) and (b) 44 g/L $Na_2SO_4$ solutions [40]. The images were captured after 4 wet-dry cycles and each cycle duration was one month. From left to right 3%, 5%, and 8% $Na_2B_4O_7$ LS geopolymer samples with two samples from each group marked as A and B (combined only).

**Table 4**
Microstructural properties of LS geopolymer from different literatures.

| Ref. | Tests | Summary of the findings |
|---|---|---|
| Liu et al.[48] | SEM | revealed composite textures of N(C)-A-S-H gel and various crystals like quartz, anhydride, sodium sulfate, and sodium hydroxides, embedded within the gel matrix and acting as fine aggregates. |
| | XRD | showed more pronounced 'hump' peaks for the specimens heat-activated at higher temperatures, indicating an increase in active amorphous phases and the presence of new crystals like sodium sulfate due to the dissolution of sulfate ions from cracked anhydride. |
| | FT-IR | identified characteristic peaks associated with quartz, octahedral alumina, and single ring vibrations in aluminosilicate, along with a peak at 443 $cm^{-1}$, suggesting the presence of Si-O-Si ($SiO_4$ tetrahedra) deformation vibrations. |
| Liu et al.[36] | SEM | the surface of LS particles became rough and loose after being cracked by alkaline hydrolysis, facilitating the formation of N(C)-A-S-H gel which precipitated on the surface of LS particles, indicating significant changes in the microstructure over time |
| | XRD | disappearance of the gypsum peak and the gradual disappearance of the peak of leached spodumene in a highly alkaline solution, followed by the appearance of a zeolite-like phase and a broad hump indicating the presence of N(C)-A-S-H gel, suggesting significant mineralogical changes over time |
| | FT-IR | increasing O-H group vibration over time, indicating the presence of amorphous gel and hydroxysodalite, with peaks associated with quartz, octahedral alumina, and single-ring vibration in aluminosilicate, reflecting changes in the interlinkages within the aluminosilicate gel |
| Karrech et al.[49] | SEM | LS particles of 50% LS and 50% GGBFS mix effectively bridge the gaps between large sand grains, leading to more effective pore refinement and finer, shallower microcracks than in other mixes, which suggests improved binding efficiency and mechanical integrity |
| | XRD | 50% LS and 50% GGBFS mix showed the formation of C-S-H gels, visible as a broad peak between 29° and 30° in the 2θ range, which is a crucial factor in the hardening process and directly correlates with the compressive strength of the geopolymer |
| Lemougna et al.[70] | SEM | 90% QFS and 10% LDS mix shows relics of Quartz Feldspar Sand (QFS) and Ladle Slag (LDS) particles with well-marked boundaries and minimal material melting, indicating low sintering reactions between particles due to the composition's lower sodium content |
| | XRD | 90% QFS and 10% LDS demonstrate a reduction in the crystalline reflections of quartz, which is indicative of the formation of an amorphous phase within the mix, influenced by the presence and proportion of sodium in the system |
| Wang et al.[40] | SEM | the geopolymer mortar revealed a similar density across samples but an increased number of cracks in samples with higher modulus activators, suggesting that higher modulus may lead to more significant shrinkage and cracking during curing |
| | XRD | the presence of quartz, thenardite, spodumene, and lithium aluminum silicate in the geopolymer paste, indicating a complex mineralogical composition influenced by the type of alkali-activators used |
| Luo et al.[43] | SEM | 20% LS mix show hydration products of the LS and GGBFS on the surface, indicating a partial reaction and formation of a microstructure that contributes to the material's mechanical properties |
| | XRD | 20% LS mix at 28 days reveal the mineralogical phases present in the geopolymers, indicating the extent of the reaction and the formation of analcime and AFt crystalline phases that impact the material's strength and durability |
| | FT-IR | 20% LS mix shows the characteristic absorption peaks related to the geopolymerisation reaction, providing insights into the chemical changes and formation of Si-O and C-O bonds within the geopolymer matrix indicating carbonation of the samples |
| Shah et al.[41] | SEM | geopolymer paste at 28 days of curing display different quantities of unreacted precursors and geopolymer gel for different mixes, reflecting the degree of reaction and the development of the geopolymer matrix |
| | XRD | the geopolymer mixes at both 3 days and 28 days indicate the mineralogical transformations of C-S-H and N-C-A-S-H occurring within the geopolymers, revealing insights into the extent of the geopolymerisation process and the stability of the formed phases |
| | FT-IR | O-H, Si-O-T (Si/Al), and C-O chemical functional groups indicated N-A-S-H bonding structure within the geopolymer, indicative of the ongoing chemical changes and the formation of the geopolymer matrix |
| Karrech et al.[50] | SEM | 20% LS (SS:SH = 2) showed a well-developed microstructure with visible geopolymer gel formation and a more refined and uniform texture compared to other mixes, indicating effective geopolymerisation and potential enhancement in mechanical properties |
| | XRD | 20% LS (SS:SH = 2) showed the characteristic peaks of the geopolymer phases, indicating the successful formation of geopolymer compounds and hinting at the structural integrity and strength of the mix |
| Li et al.[42] | SEM | at 7 days, the matrix structure of the geopolymer was relatively loose with visible cracks and interfaces, and at 180 days, the geopolymer surfaces were fully covered by fibrous N-A-S-H, indicating advanced pozzolanic activity of LS, which contributes to the mechanical properties of the geopolymer |
| | FT-IR | at 28 and 180 days showed absorption peaks corresponding to O-H, H-O-H, Si-O, and Al-O bonds, indicating ongoing hydration and the highest reaction degree was observed in the at 180 days. |
| Shen et al.[135] | SEM | uncompacted amorphous gels were observed to attach to unreacted particles, forming a loose gel network and samples with high active precursors showed more homogeneous and dense morphological characteristics, with optimization in the compactness of matrix and pore distribution in 50% LS mix |
| | XRD | incorporation of SF and SG resulted in the broadening and weakening of diffraction peaks, indicating different depolymerization degrees of silicate structures affected by synergic and coupling relationships between precursors |
| | FT-IR | shift in the Si-O-T (tetrahedral Si or Al) stretching vibration bands was observed, suggesting the reconstruction of the silicate framework during geopolymerisation and the formation of new amorphous aluminosilicate gels |
| Javed et al.[44] | SEM | higher dissolution of sulfate content in the geopolymer paste matrix induced the cracking and disintegration in N-(C)-A-S-H gel |
| | XRD | identified and quantified the zeolite-based aluminosilicate crystals from Rietveld quantitative analysis and amorphous phase in geopolymer paste does not correspond with the compressive strength development of geopolymer pastes |
| Shen et al.[137] | SEM | the pore size of geopolymer foams increased with the dosage of Al powder, and pore partition matrix revealed compacted gels acting as binders and refining the pore structure by forming crystalline N(C)-A-S-H phases |
| | XRD | increase in Al powder dosage, no significant newly crystalline phases were detected, confirming the presence of typical diffuse humps corresponding to amorphous aluminosilicate gels. |
| | FT-IR | the Si-O-T bands, with slight changes in band area and shape when reclaimed materials were introduced, indicating a negative effect on the formation of polymeric silicates |
| Fan et al.[38] | SEM | samples with different heavy metals demonstrated that the incorporation of these metals had distinct effects on the geopolymer's microstructure |

(*continued on next page*)

**Table 4** (*continued*)

| Ref. | Tests | Summary of the findings |
|---|---|---|
| | XRD | heavy metals incorporated LS geopolymer produce new diffraction peaks, but did not affect the type of hydration products C-(A)-S-H (Tobermite) and N-A-S-H (Albite), but the intensity of the main diffraction peaks of N-A-S-H was weakened after heavy metal incorporation |
| | FT-IR | absorption peaks associated with O-H stretching and bending vibrations, Al-O bending vibration, Al-O-Si symmetric stretching vibration, and Si-O-Si bending vibration were not altered by the addition of heavy metals |
| Luo et al.[47] | SEM | samples with NaOH and $Ca(OH)_2$ or NaOH and $CaCO_3$ as activators, a higher degree of hydration was observed with well-cemented hydration products, indicating a more compact structure and higher mechanical properties |
| | XRD | diffuse peaks related to N-A–S–H and C-A–S–H gels were observed, with the diffraction peak areas of these gels being roughly the same across samples, suggesting a similar gel formation irrespective of the activator used |
| | FT-IR | samples contained more bound water, and more C-A–S–H gels were generated, as evidenced by the characteristic absorption peaks of the $[CO_3]^{2-}$ ion |
| Dai et al.[46] | SEM | showed a dense granular disorderly accumulation of connections on the solidified body's surface with a small number of pores and the granular gel products observed in the fracture section indicated that the gel changed the microstructure of the solidified body by covering, bonding, and filling the pores between the incompletely activated tailings |
| | XRD | the geopolymer had a split diffraction feature peak and indicating the presence of both crystalline and amorphous phases in the sample |
| Guo and Wang [136] | SEM | Higher LS in geopolymer mix may reduce the overall active silicon-aluminum phase content in the AAM paste, resulting in a decrease in C-(A)-S-H gel content |
| | XRD | Peaks of C-A-S-H, hydrocalcite, and hydrogen aluminum silicate formation provided strength development of LS geopolymer |
| | FT-IR | high bands occurring at 983 $cm^{-1}$ are related to the stretching vibration of Si-O-Si (Al) group from C-(A)-SH and indicating that the gel network |

Here, QFS, SG, and ISW represent quartz and felspar rich lithium mine tailings, slag, and industrial solid wastes, respectively.

mass changes when exposed to solutions of 44 g/L $Na_2SO_4$ and 5 g/L $MgSO_4$. They conducted this experiment over four wet-dry cycles, each lasting one month. The findings are depicted in Fig. 6, showing the sulfate attack on 3–8% $Na_2B_4O_7$ samples in both $MgSO_4$ and $Na_2SO_4$ solutions. The data indicate that the compressive strength reduction for 3–5% $Na_2B_4O_7$ LS mixes in $MgSO_4$ solution was 0.23–5.21% less than in $Na_2SO_4$, as shown in Fig. 6(a). Conversely, the 8% $Na_2B_4O_7$ LS mix showed a 1.33% higher strength loss in $MgSO_4$ compared to $Na_2SO_4$. Moreover, LS geopolymers displayed more mass loss in $Na_2SO_4$ wet-dry cycles, as $Na_2SO_4$ more rapidly diminishes the alkaline environment than $MgSO_4$, as evidenced in Fig. 6(b). However, assessing the compressive strength of sulfate-attacked samples provides valuable insights into the sulfate resistance of LS geopolymers [169]. Generally, $MgSO_4$ solutions are more corrosive due to the formation of brucite and M-S-H. However, in this study, the $MgSO_4$ concentration was lower at 5 g/L compared to $Na_2SO_4$. Consequently, highly concentrated $Na_2SO_4$ exposed samples experienced quicker formation of ettringite or secondary ettringite from available gypsum and C-S-H, leading to greater mass and strength deterioration.

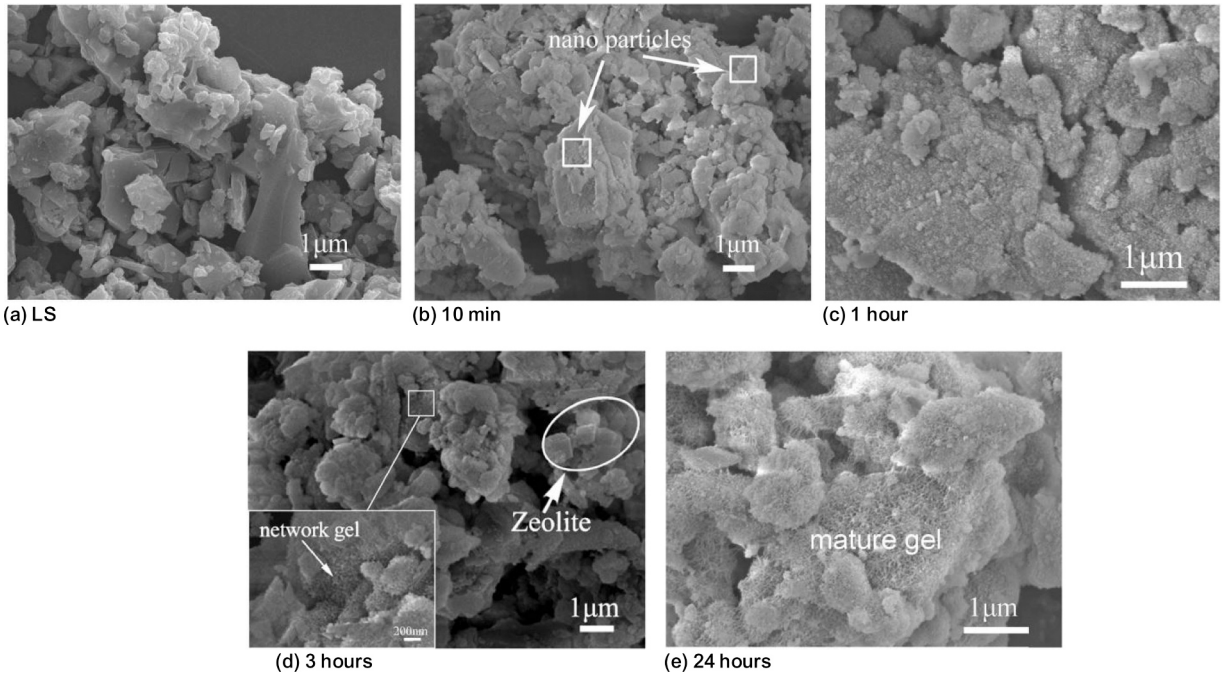


**Fig. 7.** Development of zeolite network gel in LS geopolymer at 10 min, 1 h, 3 h, and 24 h [36]. (combined only).

## 7. Microstructural properties

### 7.1. SEM

In discussing the research findings on SEM by different studies as outlined in Table 4 and comparing them with the mix design from Table 1 and the compressive strength results from Table 3, we observe a progression in understanding the microstructural properties of geopolymer mixes and their impact on mechanical properties. Liu et al. [36] investigated the microstructural properties of LS as shown in Fig. 7(a), and discussed the effects of alkali activation on LS geopolymer. The study discussed the alkaline hydrolysis causes porous microstructure and cracks after 10 min of reaction with different modulus of activators, as shown in Fig. 7(b). The oligomers are formed after one hour from the release of silicate and aluminate of active aluminosilicate in LS, as depicted in Fig. 7(c). Later, zeolite phases were detected through the polycondensation of silicate and aluminate after three hours of reaction, as shown in Fig. 7(d). The zeolite phases and oligomers together form a mature gel network by forming N-(C)-A-S-H gel that governs the interparticle gap of

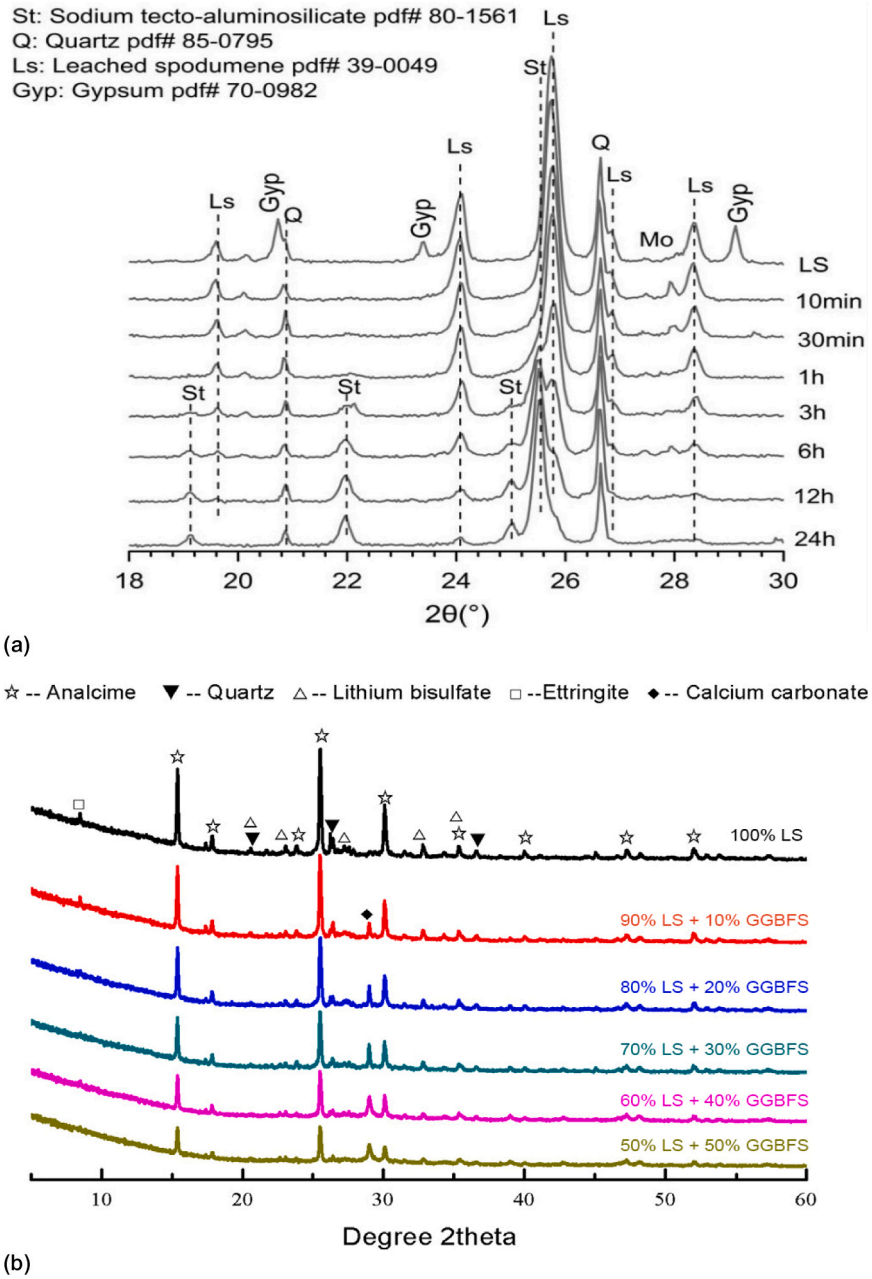


**Fig. 8.** XRD Pattern of LS geopolymer at early hydration [36] (a) and GGBFS incorporated LS geopolymers (b) [43].

products at one day of curing, as shown in Fig. 7(e) [36]. The compressive strength was 12.9 MPa at 7 days and 12.8 MPa at 28 days, suggest that the mechanical properties were maintained over time due to the formation of stable microstructural phases in the geopolymer.

In a different study Liu et al. [48] investigated an alkali-activated LS geopolymer treated at varying heating temperatures of raw, 500, and 700°C. Calcined LS geopolymers form a higher amount of N-(C)-A-S-H gel and formed dense microstructure at an early age, as quartz, anhydride, sodium sulfate, and sodium hydroxides embedded in the gel matrix [48]. However, the formation of cracks is ascertained with different factors such as activator modulus, curing temperature, binder content, and physiochemical properties of the binder. In particular, mixtures with a higher modulus of activator showed higher microcracks during curing phase. Karrech et al. [49] found that a high content of LS particles bridged the gaps between the large sand grains, and microcracks started from the interfacial transition zone (ITZ) to surrounding particles. More effective pore refinement occurs with the partial replacement of LS by GGBFS. Specimens with 50% LS with 25% GGBFS and 25% FA showed less effective pore refinement compared to the samples with 50% LS with 50% GGBFS, and the gap between sand grains were fills by C-A-S-H gel or N-A-S-H gel, developing strength of the geopolymer. Luo et al. [43] showed SEM of 50% GGBFS LS geopolymers at 28 days and found a strong morphology with activator modulus 2.0 than 1.5 and 2. A large amount of hydrated LS and GGBFS provided denser structure and filled ITZ pores.

Shah et al. [41] showed that optimum replacement of LS by GGBFS improved the microstructure. The unreacted LS and GGBFS particles generate a small amount of C-A-S-H for a 10% substitution of LS. The amount of geopolymer gel subsequently increased with 20–40% LS replacement with GGBFS which was beneficial for the strength development and pore refinement. Other studies in Table 4, would have similarly contributed to the understanding of how various mix designs and curing processes influence the microstructure and, consequently, the mechanical strength of geopolymers. The SEM analyses across these studies highlight the characteristic changes in the composition and processing conditions can lead to variations in the microstructure, which are crucial for defining the mechanical properties and overall performance of the geopolymer composites. The SEM study highlighted the importance of complex interplay between geopolymer composition, hydration products, curing conditions, and strength development. This illustrates the adjustments in the mix design can lead to significant changes in the microstructure of the geopolymer and impacts the geopolymer's strength development and durability.

### 7.2. XRD

Liu et al. [36,48] investigated the XRD pattern of early and long-term products of alkali-activated LS geopolymer at different thermal treatments and aging, as given Fig. 8(a). The authors found the presence of sodium tecto-aluminosilicate, quartz, leached spodumene, and gypsum at the early stage of geopolymerisation [36]. Initially, after 10 min of mixing, the peak of gypsum and leached spodumene gradually disappeared due to dissolution in LS and highly alkaline solution. Later, a zeolite-like phase was formed, and a broad hump at 15–40° 2-θ was noticed at 3 h, which indicates the presence of amorphous N-(C)-A-S-H gel in a regular network. The presence of zeolite phases may subsequentially result in the peak of sodium tecto-aluminosilicate in the XRD pattern presented in Fig. 8 (a). However, the authors found spodumene, lithium aluminosilicate, quartz, stishovite, anhydrite, gypsum, and hemihydrate gypsum in the hydrated LS geopolymers [48]. A broad hump at 15–50° 2-θ in LS geopolymer was noticed when treated at 500 and 700°C referred to formation of more amorphous gel [48]. The presence of anhydride and new crystal of $Na_2SO_4$ was noticed in the XRD pattern due to the dissolution of $SO_4^{2-}$ from cracked anhydride.

Karrech et al. [49] discussed the XRD patterns of geopolymer products containing 50% GGBFS LS geopolymer on 3 and 28 days. Later, Luo et al. [43] investigated the XRD patterns of similar mixes for 28 days. Karrech et al. [49] explained C-S-H gel formation at 28 days with a broad peak of 29–30° 2-θ. This referred to the development of compressive strength which was increased by 34.2 MPa between 3 and 28 days of curing. The author also compared specimens containing 50% GGBFS with 50% FA, 50% kaolin, and 50% metakaolin. At 3 days, the samples with LS had the lowest hardening rate compared to other mixes. The sample containing kaolin exhibited a relatively flat peak of C-S-H gel. Specimens containing 50% GGBFS and 50% FA, and 50% GGBFS and 50% metakaolin showed compressive strengths of 48.2 and 48.7 MPa, respectively, while 50% GGBFS and 50% LS developed lower compressive strength of 31.4 MPa at 3 days curing age. The samples containing 50% LS developed the higher peak of C-S-H, which matches with the XRD pattern of other mixes at 28 days of curing [49]. Luo et al. [43] found an improvement of 20.3 MPa in compressive strength by increasing GGBFS content in the specimens. Higher GGBFS content expediates the formation of higher amount C-S-H gel at 28 days compared to 3 days. The major mineral phases were analcime ($NaAl(SiO_3)_2{\cdot}H_2O$), quartz ($SiO_2$), lithium bisulfate ($LiHSO_4$), ettringite, and calcium carbonate ($CaCO_3$) as presented in Fig. 8(b). The crystalline peak of $CaCO_3$ is more evident in the hydration products as activated GGBFS produced by carbonation [43].

The LS geopolymer can formed crystalline phases such as gypsum, quartz, lithium aluminosilicate, and calcium carbonate that facilitate to form N-(C)-A-S-H gel [43,48,49]. The progression of these studies highlights the vital role of XRD in understanding the crystalline structure of geopolymers. The transition from crystalline to amorphous phases, as detected by the XRD, is a crucial factor in determining the mechanical strength and durability of these materials. It highlights how changes in mix composition, such as the type of precursors and activators used, as well as the curing conditions, can significantly alter the crystalline structure, thereby affecting the material's properties. Overall, the chronological discussion of these XRD findings, in conjunction with the mix design and compressive strength data, paints a comprehensive picture of the intricate relationship between the microstructural characteristics and the mechanical performance of geopolymer mixes. This relationship is pivotal in optimizing geopolymer formulations for specific applications, ensuring both structural integrity and sustainability.

### 7.3. Fourier-transform infrared spectroscopy (FT-IR)

FT-IR provides a further investigation of the microstructural characteristics of LS geopolymer. FT-IR also helps distinguish the absorption bands' characteristic pattern and identifies chemical bonding to provide a quantitative product formation of LS geopolymer concrete. Luo et al. [43] performed an FT-IR analysis of LS-based geopolymer containing 0–50% GGBFS as a partial replacement. The high volume of GGBFS intensifies H-O-H asymmetric vibrations at 3400 $cm^{-1}$, as depicted in Fig. 9. The authors explained that higher undulation of H-O-H indicates that higher mass of water retained in the capillary and gel pores of the specimens. Besides, high GGBFS content proportionally increases the absorption peak of C-O asymmetric vibrations wavelength at 1417 $cm^{-1}$, which indicates carbonation [170]. Also, the asymmetric vibration at 714 and 875 $cm^{-1}$ provided by $CO_3^{2-}$ and a similar carbonation phenomenon were concluded. Apart from bound water and carbonations, some authors included forming N(C)-A-S-H gel and Si-O-Si to Si-O-Al based on the vibration intensity at a wavenumber near 950 to1100 and 979 $cm^{-1}$, respectively [170,171].

Shah et al. [41] discussed the presence of $SiO_4^{2-}$ tetrahedral deformation, O-H stretching, and H-O-H group centre at the absorption peaks near 453 $cm^{-1}$, 1640 $cm^{-1}$, and 3450 $cm^{-1}$, respectively. In contrast, Wang et al. [40] stated that different alkali dosages with a similar activator modulus did not significantly affect water bonding. FT-IR analysis suggested geopolymer gel's development in forming Si-O-T (Si/Al) bonds when the vibration was adjusted between 800 to 1200 $cm^{-1}$ [43,172].

Liu et al. [36] discussed the occurrence of the absorption peak at 3500 to 3400 $cm^{-1}$ due to O-H groups in the water molecules. They resulted in the formation of amorphous gel and hydroxy consolidation with time. In addition, the peak around 1634 $cm^{-1}$ was assigned to the stretching vibrations generated by the O-H bonds. The vibrations resulted from the absorbed $H_2O$, hydroxides, or hydrates. Typical adsorption of Si-O-T (Si/Al) asymmetric stretching vibrations considered to be the formation of N(C)-A-S-H gels were identified between the peaks at 1300 and 1000 $cm^{-1}$ [173–175]. In addition, the authors assumed that asymmetric vibration of 950 to 1200 $cm^{-1}$ resulted from the resonance of Si-O-Si or Si-O-Al and O-Si-O band in the environment. In conclusion, different literatures also specified some other absorption peaks at the wavelength 1000 $cm^{-1}$, 778 to 796 $cm^{-1}$, 725 $cm^{-1}$, and 550 to 560 $cm^{-1}$ indicating the presence of double bands in N-A-S-H gel, quartz, alumina, and single ring vibration in aluminosilicate [43,173,176–178].

## 8. Leaching of heavy metals

Fan et al. [38] provided extensive insights into heavy metal leaching from MK-NS-LS ternary geopolymer and the study reported that leaching concentrations of Pb, Cr, and Cu were far below hazardous limits, and decreased over time, indicating effective immobilization within the geopolymer matrix. Different pH environments showed varying effects on the leaching patterns of these metals. The study also analysed the chemical forms of these metals, revealing that most of them were in a residual form, which poses minimal environmental risk. Fan et al. [38] demonstrated the immobilization mechanisms for heavy metals, showing that the interaction between heavy metals and the geopolymer matrix is complex and varies with the type of metal, as shown in Fig. 10. Specifically, Cu, Pb, and Cr can physically encapsulate in the hydration products through adsorption, as shown in Fig. 10 (a). On the

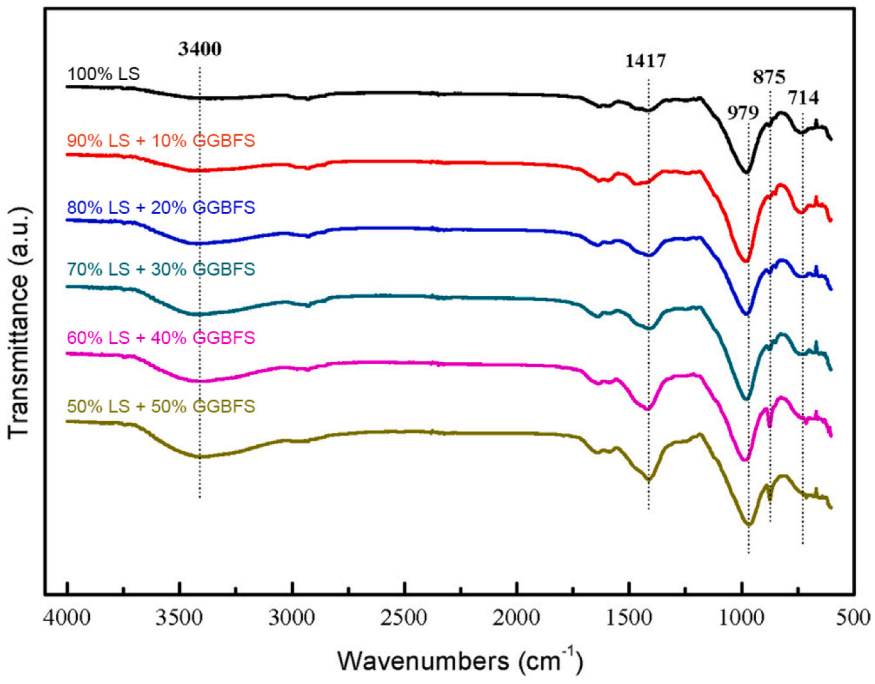


**Fig. 9.** Comparisons in FT-IR of one part LS geopolymer with partial replacement of GGBFS [43].

other hand, Cr mainly use chemical bonding to immobilise within the hydration product, as shown in Fig. 10 (b). This aligns with the findings from the different studies on heavy metal immobilisation with hydration products [179–181] and highlighting the potential of geopolymers as a sustainable solution for immobilizing heavy metals in industrial waste materials. Fan et al. [38] also discussed the porosity and microstructure of the samples, showing that heavy metal incorporation, particularly Cr, significantly altered the pore structure and impacted compressive strength and leaching behaviour. Furthermore, the XRD and FT-IR analyses suggested that heavy metal addition did not significantly change the type of hydration products but affected their intensity and structure, implying changes in the dissolution of raw materials and the immobilization mechanism of heavy metals.

Dai et al. [46] conducted leaching tests on geopolymers synthesized from LS and LZT. The leaching concentrations of various heavy metals like As, Cr, Cd, Pb, Zn, Cu, Mn, and Ba were measured and found to meet the limits required by GB 5085.1 [182]. The leaching rate was closely related to the raw materials used and the curing method and suggesting that the composition and processing of geopolymers are key factors in controlling heavy metal leaching. On the other hand, Lemougna et al. [70] and Shen et al. [137]

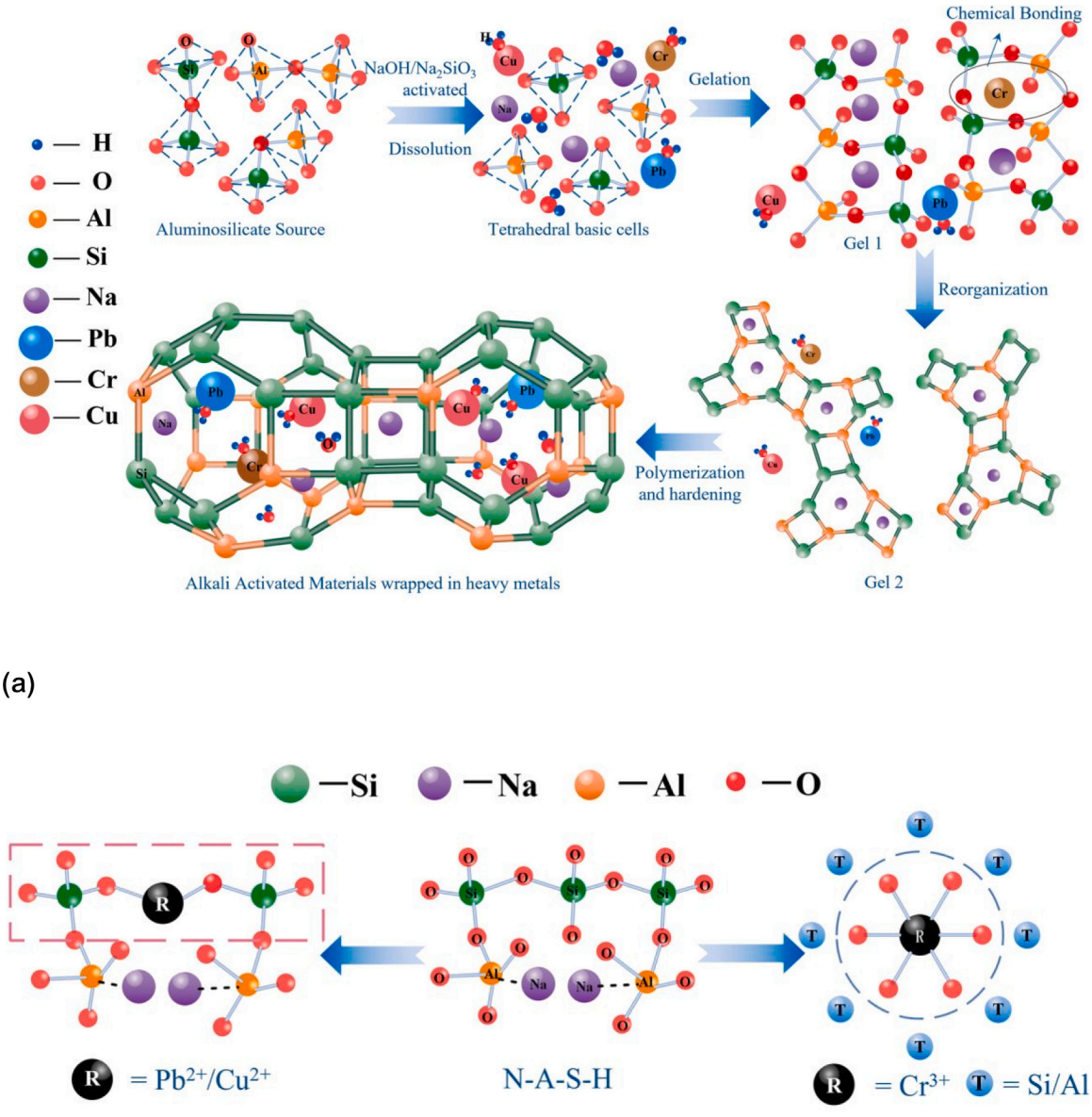


**Fig. 10.** Physical immobilisation of Cu, Cr, and Pb in MK-NS-LS ternary geopolymer (a) and (b) Chemical bonding of Cu, Cr, and Pb with N-A-S-H gel [38].

reported that negligible concentrations of Cr and Zn present in LS and the radioactive nuclei levels were very low compared to threshold limit, therefore using LS can be conveniently used as a building material. Comparing the findings from these studies, we observe a consistent theme of effective heavy metal immobilization within geopolymer matrices. The variability in leaching behaviour depending on pH and the type of heavy metal suggests complex interactions within the geopolymers. The consistent observation across studies is the transformation of heavy metals into more stable and less leachable forms within the geopolymers, reducing their environmental impact.

## 9. Conclusions

This paper has comprehensively reviewed the physio-chemical properties of LS and its characterization through various physical, thermal, and chemical processing methods. The review identifies future directions and methodologies for producing lithium slag (LS) geopolymer and discusses the mechanical, durability, and microstructural properties to understand of the LS geopolymer production process, products, and behaviour. The key findings of the study are:

- The larger mean particle size, lower specific surface area, higher volume of flaky particles, lower CaO, and higher $SO_3$ content of LS compared to conventional aluminosilicate materials present challenges in geopolymerisation. However, thermomechanical and alkali activation techniques have been effectively employed to activate LS for geopolymerisation with binary/ternary precursors combinations.
- The fresh properties of LS geopolymer are greatly influenced by workability parameters, with early stiffening occurring due to the early activation of a high volume aluminate phase. This can be mitigated with borate and appropriate dosages of retarder and activator modulus.
- LS geopolymers containing 50-70% LS combined with materials like fly ash (FA), metakaolin, kaolin, silica fume, and ground granulated blast furnace slag (GGBFS) have shown rapid gains in compressive and flexural strengths.
- The use of 20-30% GGBFS satisfactorily reduces drying shrinkage, efflorescence, and water absorption in LS geopolymers. Ternary blended FA, GGBFS, and LS composite geopolymers also show promising fresh, mechanical, durability, microstructural, and heavy metal immobilisation performance.

Therefore, while the LS and different slag combined geopolymer contributes significantly to strength development and microstructure optimisation, the broader application and development prospects of LS geopolymer in sustainable construction present exciting avenues for future research and practical applications.

## 10. Recommendations for future works

This section of the paper outlines several key areas for further research in the field of LS geopolymers. The recommendations focus on exploring various aspects to enhance the understanding and application of LS in sustainable construction. The recommendations for future works are outlined below:

- The investigation on the LS particle packing with binary/ternary precursors using laser particle size analysis and micro-computed tomography can be explored. This will clearly explain the impact of LS particle geometry on hydration, workability, strength, durability, and microstructure.
- A comprehensive investigation on workability by tests like mini-slump flow, concrete slump and air content at varying LS content levels and activator dosages needs to be conducted.
- The LS geopolymer's chemical reactivity through conductivity measurements and efficiency in removing specific ions ($Ca^{2+}$, $OH^-$, $Na^+$, $K^+$) will provide the understanding on the activation energy of LS in comparison to commonly used pozzolans.
- Future research on LS geopolymer can be incorporated with the production of self-consolidating concrete and the assessment of fresh, mechanical, durability, and microstructural properties, this will reduce the energy required for the compaction of the LS geopolymer concrete.
- The lithium concentration in the LS was reported as 1875 mg/kg [38] and the effect of Li ions in the geopolymer reaction products, durability and microstructure still needs researchers attention. The effects of acid treatment and micronisation on LS geopolymer properties can be investigated.
- The mechanical properties like compressive, tensile, flexure, and elasticity modulus of the LS geopolymer concrete can be evaluated for different mixing conditions and comparing with standards like ACI 318 [183], CEB-FIB [184], and AS 3600 [185] to promote applications in construction sector.
- The LS geopolymer concrete can be tested for split Hopkinson pressure bar, wear loss, toughness, and impact resistance for the application in the road base applications. The use of LS geopolymer concrete in the production and performance exploration of structural behaviour of the building components still unexplored.
- The durability tests including rapid chloride permeability, water permeability, and resistance to various environmental factors like, alkali-silica reaction, corrosion, carbonation, acid/salt attack, creep, and fire resistance can be investigated for the practical application of LS geopolymer concrete.
- The use of LS geopolymers in 3D concrete printing by optimizing factors like activator modulus and superplasticizer content need to be explored.

- The microstructural investigation of the ITZ of the LS geopolymer concrete through atomic force microscopy can be conducted. The LS and LS geopolymers can be analysed in Field Emission Scanning Electron Microscopy (FESEM) coupled with Electron Backscatter Diffraction (EBSD) to understand the crystallographic defects of the LS minerals and hydrated LS geopolymer phases. LS geopolymers can be further analysed in μCT scan to understand the pore size and its volume distribution. The LS and LS geopolymer products can be XRD pair distribution function to understand the characteristic atomic structure in the amorphous phases.
- The Life cycle assessment of LS and LS geopolymer products can provide a quantitative measure of the sustainable construction and disposal, reuse, and recycling techniques in different regions in the world.

The above recommendations aim to deepen the understanding of LS geopolymers, particularly their potential in sustainable construction, and to identify areas that require further exploration to optimize their use.

## CRediT authorship contribution statement

**Khair Snajida:** Conceptualization, Data curation, Formal analysis, Methodology, Writing – original draft. **Rahman SM Arifur:** Data curation, Methodology, Writing – original draft. **Shaikh Faiz Uddin Ahmed:** Funding acquisition, Project administration, Resources, Supervision, Writing – review & editing. **Sarker Prabir Kumar:** Supervision, Writing – review & editing.

## Declaration of Competing Interest

The authors declare that they have no known competing financial interests or personal relationships that could have appeared to influence the work reported in this paper.

## Data availability

No data was used for the research described in the article.

## Acknowledgements

This research was financially supported by the Australian Research Council (ARC) discovery project-DP200102784.

## References

[1] Canada, C.Ao. *The voice of Canada's cement industry*. 2022 [cited 2022; Available from: ⟨https://cement.ca/#:~:text=Concrete%20is%20so%20integral%20to%20our%20communities%20because,and%20resilience%20maximized%20energy%20efficiency%20via%20thermal%20mass⟩.
[2] N. Shehata, et al., Geopolymer concrete as green building materials: recent applications, sustainable development and circular economy potentials, Sci. Total Environ. 836 (2022), 155577.
[3] A.T.M. Marsh, A.P.M. Velenturf, S.A. Bernal, Circular Economy strategies for concrete: implementation and integration, J. Clean. Prod. 362 (2022), 132486.
[4] M.C. Caruso, et al., Comparative environmental and social life cycle assessments of off-shore aquaculture rafts made in ultra-high performance concrete (UHPC), Int. J. Life Cycle Assess. 27 (2) (2022) 281–300.
[5] S.A. Rahman, F.U.A. Shaikh, P.K. Sarker, A comprehensive review of properties of concrete containing lithium refinery residue as partial replacement of cement, Constr. Build. Mater. 328 (2022).
[6] M. Simoni, et al., Decarbonising the lime industry: state-of-the-art, Renew. Sustain. Energy Rev. 168 (2022), 112765.
[7] P. Fennell, et al., Cement and steel—nine steps to net zero, Nat. Publ. Group (2022).
[8] T. Strunge, P. Renforth, M. Van der Spek, Towards a business case for $CO_2$ mineralisation in the cement industry, Commun. earth Environ. 3 (1) (2022) 1–14.
[9] L. Rosa, et al., Carbon dioxide mineralization in recycled concrete aggregates can contribute immediately to carbon-neutrality, Resour., Conserv. Recycl. 184 (2022), 106436.
[10] D. Babor, D. Plian, L. Judele, *Environmental impact of concrete.* Buletinul Institutului Politehnic din lasi, Sect. Constr., Arhit. 55 (4) (2009) 27.
[11] Y. Rifaai, et al., Rheology and mechanical performance of self-consolidating hybrid-geopolymer concrete as a sustainable construction material, Constr. Build. Mater. 314 (2022), 125633.
[12] B.B. Jindal, et al., Geopolymer concrete with metakaolin for sustainability: a comprehensive review on raw material's properties, synthesis, performance, and potential application, Environ. Sci. Pollut. Res. (2022) 1–26.
[13] H.U. Ahmed, et al., Geopolymer concrete as a cleaner construction material: An overview on materials and structural performances, Clean. Mater. (2022), 100111.
[14] A. Raza, et al., A scientometric review on mechanical and durability performance of geopolymer Paste: Effect of various raw materials, Constr. Build. Mater. 345 (2022), 128297.
[15] I. Luhar, S. Luhar, A Comprehensive Review on Fly Ash-Based Geopolymer, J. Compos. Sci. 6 (8) (2022) 219.
[16] Z. He, S. Du, D. Chen, Microstructure of ultra high performance concrete containing lithium slag, J. Hazard. Mater. 353 (2018) 35–43.
[17] J. Lu, et al., Effect of lithium-slag in the performance of slag cement mortar based on least-squares support vector machine prediction, Mater. (Basel) (2019).
[18] L. Qi, et al., Influence of lithium slag from lepidolite on the durability of concrete, IOP Conf. Ser.: Earth Environ. Sci. 61 (2017), 012151.
[19] S.K. Nath, Fly ash and zinc slag blended geopolymer: immobilization of hazardous materials and development of paving blocks, J. Hazard. Mater. 387 (2020), 121673.
[20] J.L. Provis, J.S. Van Deventer, Alkali activated materials: state-of-the-art report, RILEM TC 224-AAM, Vol. 13, Springer Science & Business Media,, 2013.
[21] V. Sata, P. Chindaprasirt, 19 - Use of construction and demolition waste (CDW) for alkali-activated or geopolymer concrete, in: F. Pacheco-Torgal, et al. (Eds.), Advances in Construction and Demolition Waste Recycling, Woodhead Publishing, 2020, pp. 385–403.
[22] N.B. Singh, 19 - Fly ash in the construction industry, in: K.K. Kar (Ed.), Handbook of Fly Ash, Butterworth-Heinemann, 2022, pp. 565–610.
[23] J. Davidovits, Geopolymer, green chemistry and sustainable development solutions: proceedings of the world congress geopolymer 2005, Geopolymer Institute,, 2005.
[24] M. Amran, et al., Long-term durability properties of geopolymer concrete: an in-depth review, Case Stud. Constr. Mater. 15 (2021), e00661.
[25] M. Amran, et al., Fire resistance of geopolymer concrete: a critical review, Constr. Build. Mater. 324 (2022), 126722.
[26] M. Albitar, et al., Durability evaluation of geopolymer and conventional concretes, Constr. Build. Mater. 136 (2017) 374–385.

[27] M.A. Aleem, P. Arumairaj, Geopolymer concrete–a review, Int. J. Eng. Sci. Emerg. Technol. 1 (2) (2012) 118–122.
[28] S. Bernal, et al., Performance at high temperature of alkali-activated slag pastes produced with silica fume and rice husk ash based activators, Mater. De. Constr. 65 (318) (2015).
[29] S.K. Das, et al., Characterization and utilization of rice husk ash (RHA) in fly ash–Blast furnace slag based geopolymer concrete for sustainable future, Mater. Today.: Proc. 33 (2020) 5162–5167.
[30] H.S. Abhishek, et al., Fresh mechanical and durability properties of alkali-activated fly ash-slag concrete: a review, Innov. Infrastruct. Solut. 7 (1) (2021), 116.
[31] H. Tan, et al., Utilization of lithium slag as an admixture in blended cements: physico-mechanical and hydration characteristics, J. Wuhan. Univ. Technol. -Mater. Sci. Ed. 30 (1) (2015) 129–133.
[32] W. Mrozik, et al., Environmental impacts, pollution sources and pathways of spent lithium-ion batteries, Energy Environ. Sci. 14 (12) (2021) 6099–6121.
[33] Geoff, L., Hazardous Waste in Australia 2021: The Department of Agriculture, Water and the Environment, P. Joe and W. Christine, Editors. 2021: Australia.
[34] Centre for Collective Learning. *Electrical machinery and equipment and parts thereof; sound recorders and reproducers; television image and sound recorders and reproducers, parts and accessories of such articles*. 2020; 5.1.8:[Available from: ⟨https://oec.world/en/profile/hs/electrical-machinery-and-equipment-and-parts-thereof-sound-recorders-and-reproducers-television-image-and-sound-recorders-and-reproducers-parts-and-accessories-of-such-articles⟩.
[35] Z. He, L.-y Li, S. Du, Mechanical properties, drying shrinkage and creep of concrete containing lithium slag, Constr. Build. Mater. 147 (2017) 296–304.
[36] Z. Liu, et al., Characteristics of alkali-activated lithium slag at early reaction age, J. Mater. Civ. Eng. 31 (12) (2019).
[37] L.V. Garcia, et al., Lithium in a sustainable circular economy: a comprehensive review, Processes 11 (2) (2023) 418.
[38] J. Fan, et al., Heavy metals immobilization of ternary geopolymer based on nickel slag, lithium slag and metakaolin, J. Hazard. Mater. 453 (2023), 131380.
[39] L. Zhang, et al., Corrosion behavior of concrete fabricated with lithium slag as corrosion inhibitor under simulated acid rain corrosion action, J. Clean. Prod. 377 (2022), 134300.
[40] J. Wang, et al., Setting controlling of lithium slag-based geopolymer by activator and sodium tetraborate as a retarder and its effects on mortar properties, Cem. Concr. Compos. 110 (2020).
[41] S.F. Ali Shah, et al., Development of cleaner one-part geopolymer from lithium slag, J. Clean. Prod. 291 (2021).
[42] M. Li, et al., The effects of lithium slag on microstructure and mechanical performance of metakaolin-based geopolymers designed by response surface method (RSM), Constr. Build. Mater. 299 (2021), 123950.
[43] Q. Luo, et al., Properties and microstructure of lithium-slag-based geopolymer by one-part mixing method, Constr. Build. Mater. 273 (2021).
[44] U. Javed, F.U.A. Shaikh, P.K. Sarker, Microstructural investigation of lithium slag geopolymer pastes containing silica fume and fly ash as additive chemical modifiers, Cem. Concr. Compos. 134 (2022), 104736.
[45] U. Javed, F. Uddin, Ahmed Shaikh, and P. Kumar Sarker, Microstructural investigation of thermo-mechanically processed lithium slag for geopolymer precursor using various characterization techniques. Constr. Build. Mater. 342 (2022), 127952.
[46] B.-B. Dai, et al., Solidification experiment of lithium-slag and fine-tailings based geopolymers, Sustainability 15 (5) (2023) 4523.
[47] Q. Luo, et al., Lithium slag-based geopolymer synthesized with hybrid solid activators, Constr. Build. Mater. 365 (2023), 130070.
[48] Z. Liu, et al., A green route to sustainable alkali-activated materials by heat and chemical activation of lithium slag, J. Clean. Prod. 225 (2019) 1184–1193.
[49] A. Karrech, et al., Sustainable geopolymer using lithium concentrate residues, Constr. Build. Mater. 228 (2019).
[50] A. Karrech, et al., Delithiated β−spodumene as a geopolymer precursor, Constr. Build. Mater. 309 (2021), 124974.
[51] A. Karrech, et al., Management and valorisation of delithiated β-spodumene and its processing stream, Case Stud. Constr. Mater. 15 (2021), e00671.
[52] P. Perumal, et al., One-part geopolymers from mining residues – effect of thermal treatment on three different tailings, Miner. Eng. 144 (2019).
[53] Y. Tian, et al., Improving the rheological behavior of alkali-activated slag pastes by using low surface free energy mineral admixtures, Constr. Build. Mater. 392 (2023), 131879.
[54] J.C. Kuri, P.K. Sarker, F.U.A. Shaikh, Sulphuric acid resistance of ground ferronickel slag blended fly ash geopolymer mortar, Constr. Build. Mater. 313 (2021), 125505.
[55] M. Li, et al., The effects of lithium slag on microstructure and mechanical performance of metakaolin-based geopolymers designed by response surface method (RSM), Constr. Build. Mater. 299 (2021).
[56] S.W. Huang, et al., Study on preparing aero-concrete using leaching residual slag of lepidolite ore, Appl. Mech. Mater. 99-100 (2011) 375–378.
[57] K.B. Shi, S. Zhang, Ring method test on the early-age anti-cracking capability of high-performance lithium slag concrete, Appl. Mech. Mater. 94-96 (2011) 782–785.
[58] L.F. Zhang, R.Y. Wang, Experimental study on alkali-activated slag-lithium slag-fly ash environmental concrete, Adv. Mater. Res. 287-290 (2011) 1237–1240.
[59] H.F. Li, L. Guo, Y. Xia, Mechanical properties of concretes containing super-fine mineral admixtures, Appl. Mech. Mater. 174-177 (2012) 1406–1409.
[60] M. Haigh, et al., Development of New High Performance Supplementary Cementitious Material – A Lithium Production By-Product, in *CIA Binnual Coference*, Concrete Institute of Australia (CIA),, Australia, 2013.
[61] H. Wen, Property research of green concrete mixed with lithium slag and limestone flour, Adv. Mater. Res. 765-767 (2013) 3120–3124.
[62] W. Fu-fei, S. Ke-bin, D. Shuang-kuai, Properties and microstructure of HPC with lithium-slag and fly ash, Key Eng. Mater. 599 (2014).
[63] P.H.R. Borges, et al., Lithium aluminosilicate residue as raw material in the production of sustainable concrete masonry units: a Brazilian case, Open Constr. Build. Technol. J. 10 (1) (2016) 418–430.
[64] Y. Qiu, et al., Recycling of spodumene slag: preparation of green polymer composites, RSC Adv. 6 (43) (2016) 36942–36953.
[65] Z. He, et al., Nanoindentation Characteristics of Cementitious Materials Containing Lithium Slag, 9, American Scientific Publishers,, 2017, pp. 155–160 **(2)**(6).
[66] Z. He, et al., Effect of lithium slag on drying shrinkage of concrete with manufactured-sand, J. Residuals Sci. Technol. 14 (1) (2017) 171–176.
[67] L. Qi, et al., Influence of lithium slag from lepidolite on the durability of concrete, IOP Conf. Ser.: Earth Environ. Sci. 61 (2017).
[68] L. Chen, J. Yao, G. Zhang, Flexural properties of lithium slag concrete beams subjected to loading and thermal-cold cycles, KSCE J. Civ. Eng. 23 (2) (2018) 624–631.
[69] H. Tan, et al., Utilization of lithium slag by wet-grinding process to improve the early strength of sulphoaluminate cement paste, J. Clean. Prod. 205 (2018) 536–551.
[70] P.N. Lemougna, et al., Recycling lithium mine tailings in the production of low temperature (700–900 °C) ceramics: effect of ladle slag and sodium compounds on the processing and final properties, Constr. Build. Mater. 221 (2019) 332–344.
[71] B. Li, et al., Products and properties of steam cured cement mortar containing lithium slag under partial immersion in sulfate solution, Constr. Build. Mater. 220 (2019) 596–606.
[72] B. Munn, I. Dumitru, D. Maree, Assessment of the performance of new supplementary cementitious materials from lithium production residues. CIA Binnual Coference, Concrete Institute of Australia (CIA),, Melbourne, Australia, 2019.
[73] W. Yiren, et al., Micro-morphology and phase composition of lithium slag from lithium carbonate production by sulphuric acid process, Constr. Build. Mater. 203 (2019) 304–313.
[74] Z. He, et al., Hydration and microstructure of concrete containing high volume lithium slag, Mater. Express 10 (3) (2020) 430–436.
[75] J. Li, S. Huang, Recycling of lithium slag as a green admixture for white reactive powder concrete, J. Mater. Cycles Waste Manag. 22 (6) (2020) 1818–1827.
[76] J. Li, et al., Recycling of lithium slag extracted from lithium mica by preparing white Portland cement, J. Environ. Manag. 265 (2020), 110551.
[77] H. Tan, et al., Preparation for micro-lithium slag via wet grinding and its application as accelerator in Portland cement, J. Clean. Prod. 250 (2020).
[78] T. Zhang, et al., Effect of TIPA on mechanical properties and hydration properties of cement-lithium slag system, J. Environ. Manag. 276 (2020), 111274.
[79] Y. He, et al., Mechanical and environmental characteristics of cemented paste backfill containing lithium slag-blended binder, Constr. Build. Mater. 271 (2021).
[80] H. Tan, et al., Effect of wet grinded lithium slag on compressive strength and hydration of sulphoaluminate cement system, Constr. Build. Mater. 267 (2021).
[81] M. Zhai, et al., Hydration properties and kinetic characteristics of blended cement containing lithium slag powder, J. Build. Eng. 39 (2021).
[82] S.M.A. Rahman, et al., Fresh state and hydration properties of high-volume lithium slag cement composites, Mater. Struct. 56 (4) (2023), 91.

[83] M. Prasad, K. Reid, H. Murray, Kaolin: processing, properties and applications, Appl. clay Sci. 6 (2) (1991) 87–119.
[84] G. Kakali, et al., Thermal treatment of kaolin: the effect of mineralogy on the pozzolanic activity, Appl. clay Sci. 20 (1-2) (2001) 73–80.
[85] C.Y. Heah, et al., Effect of curing profile on kaolin-based geopolymers, Phys. Procedia 22 (2011) 305–311.
[86] A. Lotfy, et al., Effect of kaolin waste content on the properties of normal-weight concretes, Constr. Build. Mater. 83 (2015) 102–107.
[87] F.N. Okoye, J. Durgaprasad, N.B. Singh, Fly ash/Kaolin based geopolymer green concretes and their mechanical properties, Data Brief. 5 (2015) 739–744.
[88] N. Shafiq, et al., Calcined kaolin as cement replacing material and its use in high strength concrete, Constr. Build. Mater. 81 (2015) 313–323.
[89] R. Abbas, et al., Preparation of geopolymer concrete using Egyptian kaolin clay and the study of its environmental effects and economic cost, Clean. Technol. Environ. Policy (2020) 1–19.
[90] S.-Q. Li, et al., Effect of Kaolin particle size on the removal of Pb (II) from aqueous solutions by Kaolin-supported nanoscale zero-valent iron, Mater. Res. Express 7 (4) (2020), 045002.
[91] I. Slatni, et al., Mesoporous silica synthesized from natural local kaolin as an effective adsorbent for removing of Acid Red 337 and its application in the treatment of real industrial textile effluent, Environ. Sci. Pollut. Res. 27 (31) (2020) 38422–38433.
[92] S.M.Q. Taklymi, O. Rezaifar, M. Gholhaki, Investigating the properties of bentonite and kaolin modified concrete as a partial substitute to cement, SN Appl. Sci. 2 (12) (2020) 1–14.
[93] S. Wild, J.M. Khatib, A. Jones, Relative strength, pozzolanic activity and cement hydration in superplasticised metakaolin concrete, Cem. Concr. Res. 26 (10) (1996) 1537–1544.
[94] J.-T. Ding, Z. Li, Effects of metakaolin and silica fume on properties of concrete, Acids Mater. 99-M39 (2002) 393–398.
[95] C.-S. Poon, et al., Performance of metakaolin concrete at elevated temperatures, Cem. Concr. Compos. 25 (1) (2003) 83–89.
[96] H.A. Razak, H. Wong, Strength estimation model for high-strength concrete incorporating metakaolin and silica fume, Cem. Concr. Res. 35 (4) (2005) 688–695.
[97] N.M. Al-Akhras, Durability of metakaolin concrete to sulfate attack, Cem. Concr. Res. 36 (9) (2006) 1727–1734.
[98] J. Khatib, Metakaolin concrete at a low water to binder ratio, Constr. Build. Mater. 22 (8) (2008) 1691–1700.
[99] M. Arikan, et al., Properties of blended cements with thermally activated kaolin, Constr. Build. Mater. 23 (1) (2009) 62–70.
[100] E. Badogiannis, S. Tsivilis, Exploitation of poor Greek kaolins: durability of metakaolin concrete, Cem. Concr. Compos. 31 (2) (2009) 128–133.
[101] M. Narmatha, T. Felixkala, Metakaolin–the best material for replacement of cement in concrete, Int. J. Adv. Res. 4 (7) (2016) 1690–1696.
[102] S. Selmani, et al., Effects of metakaolin addition on geopolymer prepared from natural kaolinitic clay, Appl. Clay Sci. 146 (2017) 457–467.
[103] M. Thomas, J. Matthews, Carbonation of fly ash concrete, Mag. Concr. Res. 44 (160) (1992) 217–228.
[104] C.S. Poon, X. Qiao, Z. Lin, Pozzolanic properties of reject fly ash in blended cement pastes, Cem. Concr. Res. 33 (11) (2003) 1857–1865.
[105] G. Li, Properties of high-volume fly ash concrete incorporating nano-SiO2, Cem. Concr. Res. 34 (6) (2004) 1043–1049.
[106] R. Siddique, Performance characteristics of high-volume Class F fly ash concrete, Cem. Concr. Res. 34 (3) (2004) 487–493.
[107] C.D. Atiş, O. Karahan, Properties of steel fiber reinforced fly ash concrete, Constr. Build. Mater. 23 (1) (2009) 392–399.
[108] M. Limbachiya, M.S. Meddah, Y. Ouchagour, Use of recycled concrete aggregate in fly-ash concrete, Constr. Build. Mater. 27 (1) (2012) 439–449.
[109] Q. Zhao, et al., Long-age wet curing effect on performance of carbonation resistance of fly ash concrete, Constr. Build. Mater. 127 (2016) 577–587.
[110] E. Fidancevska, et al., Obtaining of dense and highly porous ceramic materials from metallurgical slag, Sci. Sinter. 35 (2) (2003) 85–91.
[111] K. Komnitsas, D. Zaharaki, V. Perdikatsis, Geopolymerisation of low calcium ferronickel slags, J. Mater. Sci. 42 (9) (2007) 3073–3082.
[112] Y.C. Choi, S. Choi, Alkali–silica reactivity of cementitious materials using ferro-nickel slag fine aggregates produced in different cooling conditions, Constr. Build. Mater. 99 (2015) 279–287.
[113] N. Lemonis, et al., Hydration study of ternary blended cements containing ferronickel slag and natural pozzolan, Constr. Build. Mater. 81 (2015) 130–139.
[114] A.K. Saha, P.K. Sarker, Sustainable use of ferronickel slag fine aggregate and fly ash in structural concrete: Mechanical properties and leaching study, J. Clean. Prod. 162 (2017) 438–448.
[115] Z. Zhang, et al., Conversion of local industrial wastes into greener cement through geopolymer technology: a case study of high-magnesium nickel slag, J. Clean. Prod. 141 (2017) 463–471.
[116] N. You, et al., The influence of steel slag and ferronickel slag on the properties of alkali-activated slag mortar, Constr. Build. Mater. 227 (2019), 116614.
[117] Q. Liu, et al., Experimental behaviors of prefabricated members made of ferronickel slag concrete, Constr. Build. Mater. 261 (2020), 120519.
[118] J.C. Kuri, M.N.N. Khan, P.K. Sarker, Fresh and hardened properties of geopolymer binder using ground high magnesium ferronickel slag with fly ash, Constr. Build. Mater. 272 (2021).
[119] E. Douglas, et al., Alkali activated ground granulated blast-furnace slag concrete: preliminary investigation, Cem. Concr. Res. 21 (1) (1991) 101–108.
[120] G. Osborne, Durability of Portland blast-furnace slag cement concrete, Cem. Concr. Compos. 21 (1) (1999) 11–21.
[121] G. Li, X. Zhao, Properties of concrete incorporating fly ash and ground granulated blast-furnace slag, Cem. Concr. Compos. 25 (3) (2003) 293–299.
[122] İ. Yüksel, T. Bilir, Ö. Özkan, Durability of concrete incorporating non-ground blast furnace slag and bottom ash as fine aggregate, Build. Environ. 42 (7) (2007) 2651–2659.
[123] L. Zhang, et al., Recovery of titanium compounds from molten Ti-bearing blast furnace slag under the dynamic oxidation condition, Miner. Eng. 20 (7) (2007) 684–693.
[124] F. Bellmann, J. Stark, Activation of blast furnace slag by a new method, Cem. Concr. Res. 39 (8) (2009) 644–650.
[125] İ.B. Topçu, A.R. Boğa, Effect of ground granulate blast-furnace slag on corrosion performance of steel embedded in concrete, Mater. Des. 31 (7) (2010) 3358–3365.
[126] H. Huang, G. Ye, D. Damidot, Effect of blast furnace slag on self-healing of microcracks in cementitious materials, Cem. Concr. Res. 60 (2014) 68–82.
[127] A.A. Aliabdo, M. Abd Elmoaty, M.A. Emam, Factors affecting the mechanical properties of alkali activated ground granulated blast furnace slag concrete, Constr. Build. Mater. 197 (2019) 339–355.
[128] S.M.A. Rahman, et al., Assessment of lithium slag as a supplementary cementitious material: Pozzolanic activity and microstructure development, Cem. Concr. Compos. 143 (2023), 105262.
[129] P.K. Choubey, et al., Advance review on the exploitation of the prominent energy-storage element: Lithium. Part I: From mineral and brine resources, Miner. Eng. 89 (2016) 119–137.
[130] Q. Yan, et al., Extraction of lithium from lepidolite by sulfation roasting and water leaching, Int. J. Miner. Process. 110-111 (2012) 1–5.
[131] L.I. Barbosa, et al., Lithium extraction from β-spodumene through chlorination with chlorine gas, Miner. Eng. 56 (2014) 29–34.
[132] U. Javed, F.U.A. Shaikh, P.K. Sarker, Microstructural investigation of thermo-mechanically processed lithium slag for geopolymer precursor using various characterization techniques, Constr. Build. Mater. 342 (2022), 127952.
[133] P. Meshram, B.D. Pandey, T.R. Mankhand, Extraction of lithium from primary and secondary sources by pre-treatment, leaching and separation: A comprehensive review, Hydrometallurgy 150 (2014) 192–208.
[134] S.F.A. Shah, et al., Improvement of early strength of fly ash-slag based one-part alkali activated mortar, Constr. Build. Mater. 246 (2020), 118533.
[135] S. Shen, et al., Explore the synergic and coupling relationships of multiple industrial solid wastes in the preparation of alkali-activated materials under different curing regimes, Mater. Today Sustainability 19 (2022), 100169.
[136] C. Guo, R. Wang, Utilizing lithium slag to improve the physical-chemical properties of alkali-activated metakaolin-slag pastes: cost and energy analysis, Constr. Build. Mater. 403 (2023), 133164.
[137] S. Shen, et al., Synthesis of industrial solid wastes based geopolymer foams for building energy conservation: effects of metallic aluminium and reclaimed materials, Constr. Build. Mater. 328 (2022), 127083.
[138] M. Criado, A. Palomo, A. Fernández-Jiménez, Alkali activation of fly ashes. Part 1: effect of curing conditions on the carbonation of the reaction products, Fuel 84 (16) (2005) 2048–2054.

[139] F. Pacheco-Torgal, J. Castro-Gomes, S. Jalali, Alkali-activated binders: a review: Part 1. Historical background, terminology, reaction mechanisms and hydration products, Constr. Build. Mater. 22 (7) (2008) 1305–1314.
[140] H. Xu, J.S.J. Van Deventer, The geopolymerisation of alumino-silicate minerals, Int. J. Miner. Process. 59 (3) (2000) 247–266.
[141] P. Duxson, et al., Understanding the relationship between geopolymer composition, microstructure and mechanical properties, Colloids Surf. A: Physicochem. Eng. Asp. 269 (1) (2005) 47–58.
[142] E.C. Bingham, Fluidity and plasticity, McGraw-Hill,, 1922.
[143] I.M. Krieger, T.J. Dougherty, A mechanism for non-Newtonian flow in suspensions of rigid spheres, Trans. Soc. Rheol. 3 (1) (1959) 137–152.
[144] J.L. Provis, A. Palomo, C. Shi, Advances in understanding alkali-activated materials, Cem. Concr. Res. 78 (2015) 110–125.
[145] F. Collins, J.G. Sanjayan, Cracking tendency of alkali-activated slag concrete subjected to restrained shrinkage, Cem. Concr. Res. 30 (5) (2000) 791–798.
[146] P. Rovnaník, Effect of curing temperature on the development of hard structure of metakaolin-based geopolymer, Constr. Build. Mater. 24 (7) (2010) 1176–1183.
[147] Nicholson, C., et al., *Novel geopolymer materials containing borate and phosphate structural units*. 2005.
[148] M. Balapour, A. Joshaghani, F. Althoey, Nano-SiO2 contribution to mechanical, durability, fresh and microstructural characteristics of concrete: a review, Constr. Build. Mater. 181 (2018) 27–41.
[149] E. John, T. Matschei, D. Stephan, Nucleation seeding with calcium silicate hydrate – A review, Cem. Concr. Res. 113 (2018) 74–85.
[150] L. Lang, N. Liu, B. Chen, Strength development of solidified dredged sludge containing humic acid with cement, lime and nano-SiO2, Constr. Build. Mater. 230 (2020), 116971.
[151] M.L. Granizo, M.T. Blanco-Varela, S. Martínez-Ramírez, Alkali activation of metakaolins: parameters affecting mechanical, structural and microstructural properties, J. Mater. Sci. 42 (9) (2007) 2934–2943.
[152] A. Nazari, A. Bagheri, S. Riahi, Properties of geopolymer with seeded fly ash and rice husk bark ash, Mater. Sci. Eng.: A 528 (24) (2011) 7395–7401.
[153] G.S. Ryu, et al., The mechanical properties of fly ash-based geopolymer concrete with alkaline activators, Constr. Build. Mater. 47 (2013) 409–418.
[154] M. Zhang, et al., A multiscale investigation of reaction kinetics, phase formation, and mechanical properties of metakaolin geopolymers, Cem. Concr. Compos. 78 (2017) 21–32.
[155] Racherla, U.S., HIGH MOSTURE RETAINING BARS COMPOSITIONS COMPRISING BORAXAS WATER STRUCTURANT in *United States Patent*. 2002: USA. p. 14.
[156] Racherla, U.S., *High moisture retaining bars compositions comprising borax as water structurant*. 2002, Google Patents.
[157] M. Hongqiang, et al., Study on the drying shrinkage of alkali-activated coal gangue-slag mortar and its mechanisms, Constr. Build. Mater. 225 (2019) 204–213.
[158] K. Kovler, S. Zhutovsky, Overview and future trends of shrinkage research, Mater. Struct. 39 (9) (2006) 827.
[159] Y. Ma, G. Ye, The shrinkage of alkali activated fly ash, Cem. Concr. Res. 68 (2015) 75–82.
[160] C.K. Yip, G.C. Lukey, J.S.J. van Deventer, The coexistence of geopolymeric gel and calcium silicate hydrate at the early stage of alkaline activation, Cem. Concr. Res. 35 (9) (2005) 1688–1697.
[161] O.A. Mohamed, Effects of the curing regime, acid exposure, alkaline activator dosage, and precursor content on the strength development of mortar with alkali-activated slag and fly ash binder: a critical review, Polym. (Basel) 15 (5) (2023).
[162] C. Ouellet-Plamondon, G. Habert, 25 - Life cycle assessment (LCA) of alkali-activated cements and concretes, in: F. Pacheco-Torgal, et al. (Eds.), Handbook of Alkali-Activated Cements, Mortars and Concretes, Woodhead Publishing, Oxford, 2015, pp. 663–686.
[163] M.Z.N. Khan, et al., Mechanical properties of ambient cured high strength hybrid steel and synthetic fibers reinforced geopolymer composites, Cem. Concr. Compos. 85 (2018) 133–152.
[164] M. Vafaei, et al., Durability performance of geopolymer cement based on fly ash and calcium aluminate cement in mild concentration acid solutions, J. Sustain. Cem. -Based Mater. 8 (5) (2019) 290–308.
[165] M. Chi, R. Huang, Binding mechanism and properties of alkali-activated fly ash/slag mortars, Constr. Build. Mater. 40 (2013) 291–298.
[166] D. Perera, et al., Disposition of Water in Metakaolinite Based Geopolymers, Ceram. Trans. 175 (2006) 225–236.
[167] J. Davidovits, Geopolymer Chemistry and Applications, Geopolymer Institute,, Saint-Quentin, 2008.
[168] S. Pangdaeng, et al., Influence of curing conditions on properties of high calcium fly ash geopolymer containing Portland cement as additive, Mater. Des. 53 (2014) 269–274.
[169] Z. Baščarević, 14 - The resistance of alkali-activated cement-based binders to chemical attack, in: F. Pacheco-Torgal, et al. (Eds.), Handbook of Alkali-Activated Cements, Mortars and Concretes, Woodhead Publishing, Oxford, 2015, pp. 373–396.
[170] G. Sun, J. Zhang, N. Yan, Microstructural evolution and characterization of ground granulated blast furnace slag in variant pH, Constr. Build. Mater. 251 (2020), 118978.
[171] M. Askarian, et al., Mix composition and characterisation of one-part geopolymers with different activators, Constr. Build. Mater. 225 (2019) 526–537.
[172] A.F. Abdalqader, F. Jin, A. Al-Tabbaa, Development of greener alkali-activated cement: utilisation of sodium carbonate for activating slag and fly ash mixtures, J. Clean. Prod. 113 (2016) 66–75.
[173] C.A. Rees, et al., In Situ ATR-FTIR study of the early stages of fly ash geopolymer gel formation, Langmuir 23 (17) (2007) 9076–9082.
[174] M. Criado, A. Fernández-Jiménez, A. Palomo, Alkali activation of fly ash: effect of the SiO2/Na2O ratio: Part I: FTIR study, Microporous Mesoporous Mater. 106 (1) (2007) 180–191.
[175] Z. Zhang, H. Wang, J.L. Provis, Quantitative study of the reactivity of fly ash in geopolymerization by FTIR, J. Sustain. Cem. -Based Mater. 1 (4) (2012) 154–166.
[176] C. Ma, et al., Properties and characterization of green one-part geopolymer activated by composite activators, J. Clean. Prod. 220 (2019) 188–199.
[177] I. Garcia-Lodeiro, et al., Compatibility studies between N-A-S-H and C-A-S-H gels. Study in the ternary diagram Na2O–CaO–Al2O3–SiO2–H2O, Cem. Concr. Res. 41 (9) (2011) 923–931.
[178] M.X. Peng, et al., Synthesis, characterization and mechanisms of one-part geopolymeric cement by calcining low-quality kaolin with alkali, Mater. Struct. 48 (3) (2015) 699–708.
[179] Z. Yunsheng, et al., Synthesis and heavy metal immobilization behaviors of slag based geopolymer, J. Hazard. Mater. 143 (1-2) (2007) 206–213.
[180] K. Komnitsas, D. Zaharaki, G. Bartzas, Effect of sulphate and nitrate anions on heavy metal immobilisation in ferronickel slag geopolymers, Appl. clay Sci. 73 (2013) 103–109.
[181] Z. Ji, Y. Pei, Bibliographic and visualized analysis of geopolymer research and its application in heavy metal immobilization: a review, J. Environ. Manag. 231 (2019) 256–267.
[182] GB 5085.1, Identification Standards for Hazardous Wastes. Identification for Corrosivity, National standard of the people's republic of China, China, 2007.
[183] ACI 318, Building Code Requirements for Structural Concrete and Commentary, Amarican Concrete Institute, Indianapolis, IN, USA, 2022.
[184] CEB-FIB, Model Code 90, in Bulletin d'information, International Federation for Structural Concrete, Switzerland, 1990, pp. 205–206.
[185] AS 3600, Concrete structures - Commentary (Supplement 1 to AS 3600:2018), Standards Australia, Australia, 2022.